ARTICLE

doi:10.1038/nature14402

Oxytocin enables maternal behaviour by balancing cortical inhibition

Bianca J. Marlin[1,2,3,4], Mariela Mitre[1,2,3,4,5,6], James A. D'amour[1,2,3,4], Moses V. Chao[1,2,4,5,6,7] & Robert C. Froemke[1,2,3,4,7]

Oxytocin is important for social interactions and maternal behaviour. However, little is known about when, where and how oxytocin modulates neural circuits to improve social cognition. Here we show how oxytocin enables pup retrieval behaviour in female mice by enhancing auditory cortical pup call responses. Retrieval behaviour required the left but not right auditory cortex, was accelerated by oxytocin in the left auditory cortex, and oxytocin receptors were preferentially expressed in the left auditory cortex. Neural responses to pup calls were lateralized, with co-tuned and temporally precise excitatory and inhibitory responses in the left cortex of maternal but not pup-naive adults. Finally, pairing calls with oxytocin enhanced responses by balancing the magnitude and timing of inhibition with excitation. Our results describe fundamental synaptic mechanisms by which oxytocin increases the salience of acoustic social stimuli. Furthermore, oxytocin-induced plasticity provides a biological basis for lateralization of auditory cortical processing.

The neuropeptide oxytocin controls social behaviours such as pair bond formation, mating and parenting[1–14]. Oxytocin is synthesized in the paraventricular nucleus (PVN) and supraoptic nucleus of the hypothalamus, and binds to a G-protein-coupled receptor with a single isoform[1,2]. Peripheral release of oxytocin is important for parturition and lactation[2,7,9], whereas central release of oxytocin appears to have cognitive effects including increased interpersonal trust and enhanced salience of socially relevant sensory input[1,3,4,6,10]. However, it remains unclear which neurons express oxytocin receptors[15,16], or how oxytocin interacts with experience to modify neural circuits and increase the salience of social information.

Here we examine how oxytocin is involved in pup retrieval, an important form of mammalian social behaviour. Mouse pups emit ultrasonic distress calls when separated from the nest, which experienced mothers (known as dams) use to locate and retrieve isolated pups[17–23]. This behaviour relies on the auditory system, as pup calls played by speakers attract maternal animals[19,21]. Physiologically, neural responses to pup calls in the mouse auditory cortex differ between dams and virgin females, with higher signal-to-noise ratios in maternal mice[23–27]. Correspondingly, most inexperienced animals do not initially retrieve pups[28]. Intriguingly, some virgin female rodents start retrieving pups after being co-housed with dam and pups or after central administration of oxytocin[7]. An ethologically important form of plasticity in the auditory cortex might therefore be enabled by oxytocin in maternal animals, allowing them to recognize the behavioural significance of infant distress calls. Here we aim to show how these neural changes occur, and what role oxytocin has in experience-dependent pup retrieval by virgins.

Oxytocin enables pup retrieval behaviour

We first determined the time course of experience-dependent pup retrieval behaviour enabled by oxytocin (Fig. 1a). Non-retrieving virgin female mice were co-housed with dams and litters, and retrieval success rates of virgins were tested over 3–7 days. Mothers were first tested to ensure that they reliably retrieved pups (Fig. 1b, d and Supplementary Video 1). Three groups of virgins were examined for pup retrieval. The first group of wild-type virgins received systemic oxytocin injections before testing (Fig. 1b–d, red). The second wild-type group received saline vehicle injections (Fig. 1b–d, black). The third optogenetic group of oxytocin-IRES-Cre mice[29,30] (*Oxt*-IRES-Cre; which express Cre recombinanse under the control of endogenous *Oxt*) expressed the channelrhodopsin-2 variant ChETA (containing a Glu123Thr mutation) in PVN oxytocin neurons, with optical fibres implanted in PVN to enhance release of endogenous oxytocin and perhaps other co-factors during retrieval testing (Fig. 1b–d, blue; Extended Data Fig. 1).

Within 12 h of being co-housed, virgin females receiving either oxytocin or optical PVN stimulation began retrieving more than saline-injected animals (Fig. 1b, c and Extended Data Fig. 2). Saline-injected virgins generally required at least 2 days of co-housing to express retrieval behaviour (Fig. 1b, c, black; Supplementary Video 2). Systemic oxytocin or optogenetic stimulation accelerated and increased retrieval, even sometimes after only a few hours of co-housing (Fig. 1b, c and Supplementary Video 3). Once retrieving, experienced virgin and dam retrieval rates and speeds were similar (Fig. 1d).

We examined retrieval in single-housed virgin females, to determine whether the effects of oxytocin required co-housing with dam and litter. Isolated virgins receiving oxytocin injections began retrieving earlier than saline-injected virgins, although slower than co-housed virgins (Fig. 1e). This demonstrates that oxytocin enables retrieval in single-housed virgins, specifically during interactions with isolated pups.

Oxytocin receptor expression is lateralized

It is unknown where in the brain oxytocin acts to improve social cognition and enable maternal behaviour. While peripheral oxytocin injections or nasal sprays have pro-social effects, it remains unclear how and where oxytocin acts on neural circuits[1,6] outside recent studies in transgenic mice[15,16]. To determine which cells express oxytocin receptors, we generated a specific oxytocin receptor antibody, OXTR-2 (Fig. 2a). The antibody labelled a subset of cells in the auditory cortex and other areas (Fig. 2b and Extended Data Fig. 3) enriched for

[1]Skirball Institute for Biomolecular Medicine, New York University School of Medicine, New York, New York 10016, USA. [2]Neuroscience Institute, New York University School of Medicine, New York, New York 10016, USA. [3]Department of Otolaryngology, New York University School of Medicine, New York, New York 10016, USA. [4]Department of Neuroscience and Physiology, New York University School of Medicine, New York, New York 10016, USA. [5]Department of Cell Biology, New York University School of Medicine, New York, New York 10016, USA. [6]Department of Psychiatry, New York University School of Medicine, New York, New York 10016, USA. [7]Center for Neural Science, New York University, New York, New York 10003, USA.

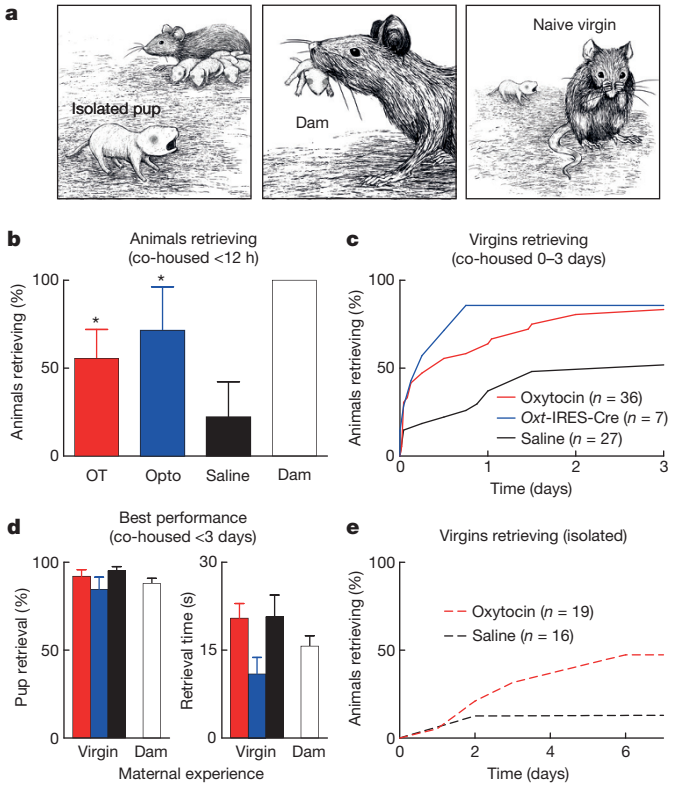

Figure 1 | Oxytocin enables pup retrieval. **a**, Retrieval behaviour. **b**, Initially naive virgins retrieving at least once <12 h after co-housing (saline: 6 out of 27 animals; oxytocin (OT): 20 out of 36 animals; $P < 0.03$, Fisher's two-tailed exact test with Bonferroni correction compared to saline; optogenetic (Opto) PVN stimulation: 5 out of 7 animals, $P < 0.05$). *$P < 0.05$. Error bars denote mean ± 95% confidence intervals. **c**, Cumulative retrieval during co-housing. **d**, Retrieval rates ($P > 0.5$, analysis of variance (ANOVA)) and speed ($P > 0.1$) were similar in dams and experienced virgins. Error bars denote mean ± s.e.m. **e**, Cumulative retrieval of saline-injected ($n = 16$) or oxytocin-injected ($n = 19$) isolated virgins (2 days after testing, saline: 2 out of 16 animals retrieved, oxytocin: 4 out of 19 animals, $P > 0.6$; 6 days, saline: 2 out of 16 animals, oxytocin: 9 out of 19 animals, $P < 0.03$).

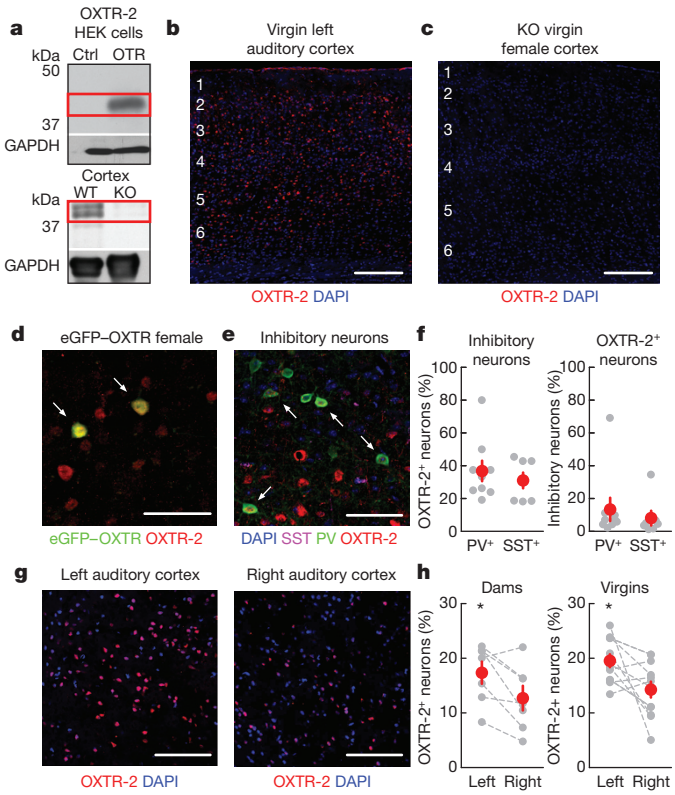

Figure 2 | Oxytocin receptor expression in female auditory cortex. **a**, Antibody to mouse oxytocin receptor (OXTR-2). Top, immmunoblot of HEK cells expressing oxytocin receptors (OTR) versus control (ctrl). Bottom, OXTR-2 immunoblots of cortical lysates from wild-type (WT) and knockout (KO) animals. Red, oxytocin receptor molecular mass (43 kilodaltons (kDa)). GAPDH was used as a loading control. **b**, Immunostaining in the left auditory cortex of naive virgin. DAPI, 4′,6-diamidino-2-phenylindole. **c**, No labelling in oxytocin receptor knockouts. **d**, Left auditory cortex of eGFP–OXTR virgin co-stained for eGFP. Arrows denote double-labelled cells. **e**, Cortical interneurons express oxytocin receptors. Virgin left auditory cortex layer 5 co-stained for parvalbumin (PV) and somatostatin (SST). **f**, Co-labelled OXTR-2^+ and PV^+/SST^+ auditory cortical cells. **g**, Left, right auditory cortex from same naive virgin. **h**, Oxytocin receptors expressed more in left auditory cortex (mothers, left: 17.4 ± 2.0%, right: 12.7 ± 2.4%, left/right asymmetry: 37.0%, $P < 0.03$, Student's two-tailed paired *t*-test, $n = 7$; virgins, left: 19.5 ± 1.2%, right: 14.3 ± 1.4%, asymmetry: 36.4%, $P < 0.02$, $n = 12$). Error bars denote mean ± s.e.m. Scale bars, 150 µm (**b**, **c**), 50 µm (**d**, **e**) and 100 µm (**g**).

oxytocin and oxytocin receptors[2,3,31]. Cells were unlabelled in oxytocin receptor knockout animals[32] (Fig. 2c and Extended Data Fig. 3). We also examined expression patterns in bacterial artificial chromosome (BAC) transgenic oxytocin receptor (OXTR)–enhanced green fluorescent protein (eGFP) mice[16,33] using antibodies to GFP (Fig. 2d). Around 30–40% of parvalbumin-positive and somatostatin-positive inhibitory interneurons expressed oxytocin receptors (Fig. 2e, f), suggesting that oxytocin is important for controlling cortical inhibition[15,16]. We also observed yellow fluorescent protein (YFP)-positive PVN axons in the auditory cortex of *Oxt*-IRES-Cre mice after viral injection, demonstrating that hypothalamic oxytocin neurons project to cortex (Extended Data Fig. 4a–c).

Notably, receptor expression in the female auditory cortex was lateralized (Fig. 2g). Significantly more cells expressed oxytocin receptors in the left auditory cortex than the right auditory cortex in mothers and naive virgins (Fig. 2h). The left auditory cortex might therefore be especially sensitive to oxytocin modulation and specialized for processing social stimuli such as pup calls. As axonal projections from PVN into cortex were not obviously lateralized (Extended Data Fig. 4d), it is likely that this anatomical specialization emerges within the cortex.

Retrieval requires the left auditory cortex

We next asked whether the left auditory cortex was functionally important for pup retrieval. We implanted cannulas into the left or right primary auditory cortex (AI) of inexperienced virgins or dams. First, we unilaterally infused the GABA agonist muscimol to inactivate the left or right auditory cortex transiently before behavioural testing. Muscimol in the left but not right auditory cortex impaired retrieval (Fig. 3a, b and Supplementary Video 4), showing that activity in the left auditory cortex is required for retrieval. These data extend an earlier study using unilateral ear plugs to show that maternal animals have right ear/left brain advantage for recognizing pup call sounds[19].

We wondered whether oxytocin within virgin left auditory cortex might accelerate expression of retrieval. Although it is unlikely that activation of a single brain area is entirely sufficient for retrieval, sensitization of the left AI might be crucial for recognizing the significance of distress calls. Animals receiving oxytocin or optogenetically stimulated in the left auditory cortex began retrieving earlier than saline-infused animals (Fig. 3c and Supplementary Videos 5 and 6). Thus, the left auditory cortex is a major component of oxytocin-sensitive circuitry for maternal behaviour.

We then asked whether oxytocin receptor activation itself was required for behavioural performance in experienced animals. We used antagonists of oxytocin receptors (OTA or L-368,899) infused into the left auditory cortex before testing retrieval in experienced

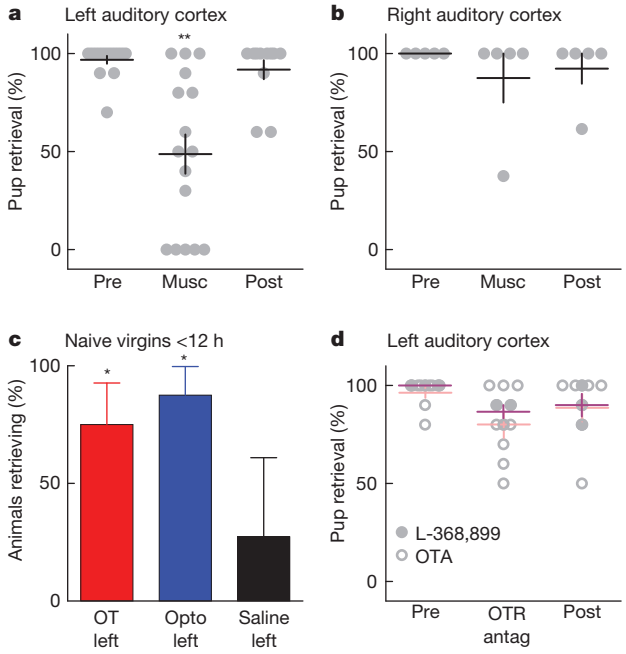

Figure 3 | Oxytocin receptors in left auditory cortex are initially required for retrieval. **a**, Muscimol infused into the left AI reduced retrieval by experienced animals (pre-muscimol retrieval: 96.9 ± 2.0%, 16 out of 16 animals retrieved at least once; muscimol: 48.8 ± 10.0%, $P < 0.002$, Fisher's one-way exact test, 11 out of 16 animals retrieved, $P < 0.025$). $^{**}P < 0.01$. Error bars denote mean ± s.e.m. **b**, Muscimol in the right AI did not impair retrieval (pre-muscimol: 100.0 ± 0.0%, muscimol: 87.5 ± 12.5%, $P > 0.9$; 5 out of 5 animals retrieved). **c**, Oxytocin in the left AI of naive virgins accelerated time to first retrieval <12 h of co-housing (oxytocin: 12 out of 16 animals, $P < 0.05$; optogenetic stimulation: 7 out of 8 animals, $P < 0.04$; saline: 3 out of 11 animals). Error bars denote mean ± 95% confidence interval. **d**, Retrieval of experienced animals with the oxytocin receptor antagonists (antag) OTA (baseline: 96.3 ± 2.6%, OTA: 80.0 ± 6.8%, $P > 0.05$; 8 out of 8 animals) or L-368,899 (baseline: 100.0 ± 0.0%, L-368,899: 86.7 ± 3.3%, $P > 0.1$, $n = 3$; 3 out of 3 animals) infused into the left AI.

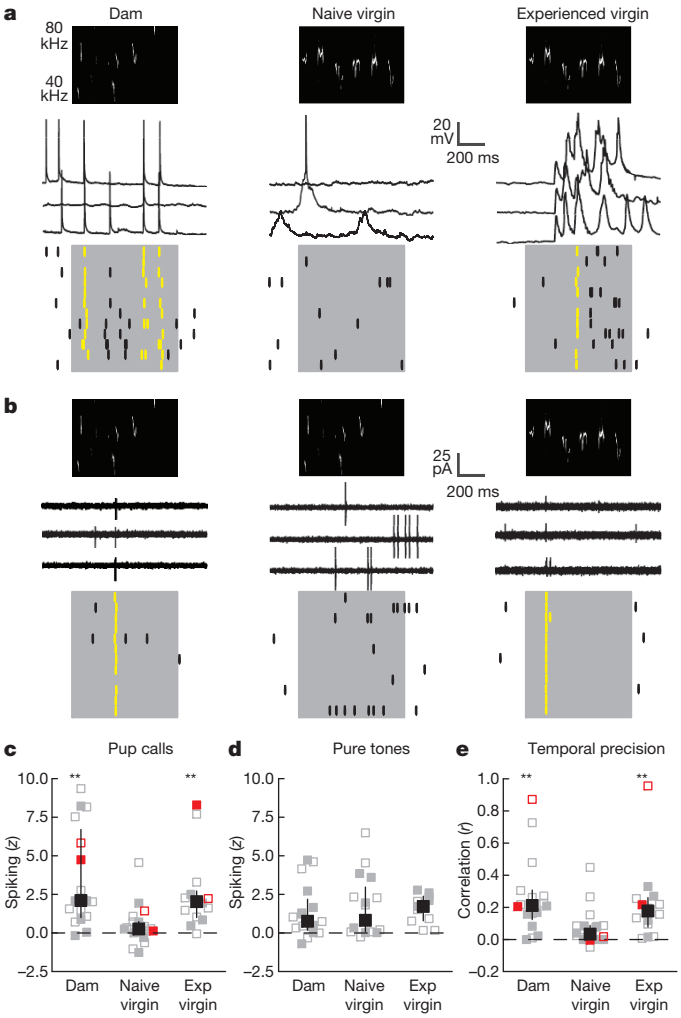

Figure 4 | Pup calls evoke reliable spikes in experienced female left AI. **a**, Current-clamp recordings in the left AI of dam (spiking *z*-score: 4.7; trial-by-trial average correlation *r*: 0.21), naive virgin (*z*-score: 0.1; *r*: −0.04), experienced virgin (*z*-score: 8.3; *r*: 0.27). **b**, Cell-attached recordings from dam (*z*-score: 5.8; *r*: 0.87), naive virgin (*z*-score: 1.4; *r*: 0.04), experienced virgin (*z*-score: 2.1; *r*: 0.96). **c**, Current-clamp (filled) or cell-attached (open) call-evoked responses in dams (black, *z*-score: 2.1 ± 1.0 (median ± s.e.m.), $n = 17$, $P < 0.0004$, $U = 288$, Wilcoxon–Mann–Whitney two-sample rank test with Bonferroni correction), naive virgins (*z*-score: 0.2 ± 0.3, $n = 20$), experienced virgins (*z*-score: 2.0 ± 0.8, $n = 14$, $P < 0.006$, $U = 240$). Error bars denote median and interquartile range. **d**, Tone-evoked responses in the left AI of dams (*z*-score: 0.7 ± 0.5, $n = 17$, $P > 0.7$, $U = 154$), naive virgins (*z*-score: 0.8 ± 0.6, $n = 17$) and experienced virgins (*z*-score: 1.7 ± 0.4, $n = 11$, $P > 0.6$, $U = 105$). **e**, Trial-by-trial correlation in dams (*r*: 0.21 ± 0.07, $n = 17$, $P < 0.002$, $U = 276$), naive virgins (*r*: 0.03 ± 0.03, $n = 20$) and experienced virgins (*r*: 0.18 ± 0.08, $n = 14$, $P < 0.012$, $U = 219$). Red symbols denote example cells shown in **a** and **b**.

animals. Neither antagonist affected performance (Fig. 3d). These data suggest that oxytocin receptors might be required only when animals first begin to retrieve, but are unnecessary for expression of retrieval behaviour thereafter (analogous to requirement of NMDA receptors for long-term potentiation induction but not maintenance). Thus, after experience with pup calls during heightened cortical oxytocin levels, changes are induced in the left auditory cortex to produce enduring memory traces for maternal behaviour.

Responses to pup calls in cortical neurons

We then asked what circuit modifications in the auditory cortex are enabled by oxytocin. Our goal was to first characterize pup call responses in single neurons from maternal animals, before determining synaptic mechanisms by which oxytocin affects the virgin brain. We used *in vivo* whole-cell recordings[34–37] to measure AI pup call responses in isoflurane-anaesthetized dams, naive virgins, and experienced virgins. In 21 current-clamp and 37 cell-attached recordings, pup calls evoked stronger responses in the left AI of mothers and experienced virgins than in naive virgins (Fig. 4a–c). As responses to pure tones were comparable across groups (Fig. 4d), differences in responsiveness between experienced and inexperienced females are specific for pup calls, not simply owing to more auditory-responsive neurons in maternal cortex. Responses in experienced females were lateralized to the left AI (Extended Data Fig. 5a, b). Notably, calls evoked precise spikes in maternal animals but not naive virgins (Fig. 4e) or the right AI (Extended Data Fig. 5a, b). We quantified temporal similarity by computing trial-to-trial cross-correlation for spiking responses, finding higher correlations in left AI neurons from experienced females (Fig. 4e and Extended Data Fig. 5b).

To examine synaptic responses to pup calls, we made 58 *in vivo* voltage-clamp recordings from AI neurons. Substantial excitatory and inhibitory postsynaptic currents (EPSCs and IPSCs) were evoked by calls in all animals. Amplitudes of call-evoked synaptic responses (Fig. 5a, b), tone-evoked responses (Fig. 5c) and spontaneous activity (Extended Data Fig. 6a–d) were comparable across groups, suggesting that reliable call-evoked spiking in maternal left AI could not be explained simply by these neurons receiving stronger excitatory inputs.

Instead, excitation and inhibition were balanced (co-tuned and precisely timed) in the left AI neurons of experienced females but

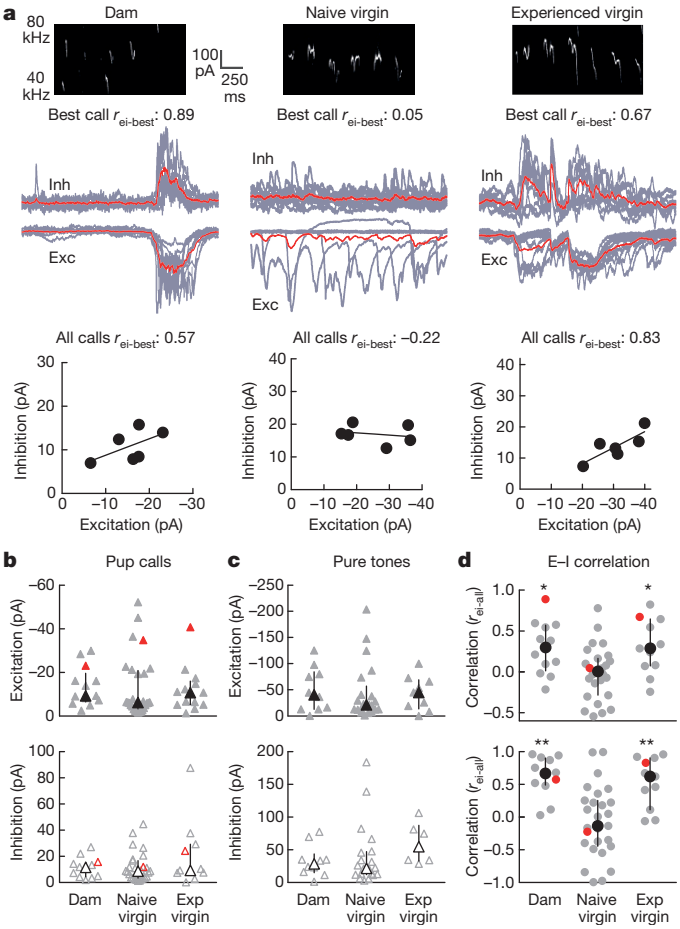

Figure 5 | Pup calls evoke correlated patterns of excitatory and inhibitory responses in left AI of experienced females. **a**, Voltage-clamp recordings from dam (top, best call responses, $r_{ei\text{-}best}$: 0.89; bottom, IPSCs and EPSCs across calls, $r_{ei\text{-}all}$: 0.57), naive virgin ($r_{ei\text{-}best}$: 0.05; $r_{ei\text{-}all}$: −0.22), experienced virgin ($r_{ei\text{-}best}$: 0.67; $r_{ei\text{-}all}$: 0.83). **b**, Synaptic call-evoked responses from dams (excitation: −9.3 ± 3.1 pA (median ± s.e.m.), $n = 13$, $P > 0.3$, $U = 229$, Wilcoxon–Mann–Whitney two-sample rank test with Bonferroni correction; inhibition: 11.6 ± 2.8 pA, $P > 0.5$, $U = 182$), naive virgins (excitation: −6.2 ± 3.3 pA, $n = 28$; inhibition: 8.7 ± 2.7 pA), experienced virgins (excitation: −10.8 ± 3.6 pA, $n = 13$, $P > 0.6$, $U = 205$; inhibition: 9.2 ± 9.5 pA, $P > 0.4$, $U = 171$). Red denotes cells in **a**. Error bars denote median and interquartile range. **c**, Tone-evoked responses in dams (excitation: −40.6 ± 16.7 pA, $n = 10$, $P > 0.4$, $U = 123$; inhibition: 28.7 ± 9.6 pA, $P > 0.7$, $U = 108$), naive virgins (excitation: −21.6 ± 14.8 pA, $n = 21$; inhibition: 21.8 ± 13.2 pA), experienced virgins (excitation: −45.2 ± 13.8 pA, $n = 9$, $P > 0.5$, $U = 107$; inhibition: 54.7 ± 16.4 pA, $P > 0.1$, $U = 92$). **d**, Excitatory–inhibitory (E–I) correlation of best call responses (top, $r_{ei\text{-}best}$) and across all calls (bottom, $r_{ei\text{-}all}$) dams ($r_{ei\text{-}best}$: 0.30 ± 0.12, $n = 12$, $P < 0.03$, $U = 245$; $r_{ei\text{-}all}$: 0.67 ± 0.11, $P < 0.0004$, $U = 278$), naive virgins ($r_{ei\text{-}best}$: 0.00 ± 0.08, $n = 27$; $r_{ei\text{-}all}$: −0.13 ± 0.13), experienced virgins ($r_{ei\text{-}best}$: 0.29 ± 0.13, $n = 12$, $P < 0.03$, U = 224; $r_{ei\text{-}all}$: 0.62 ± 0.14, $P < 0.006$, $U = 236$).

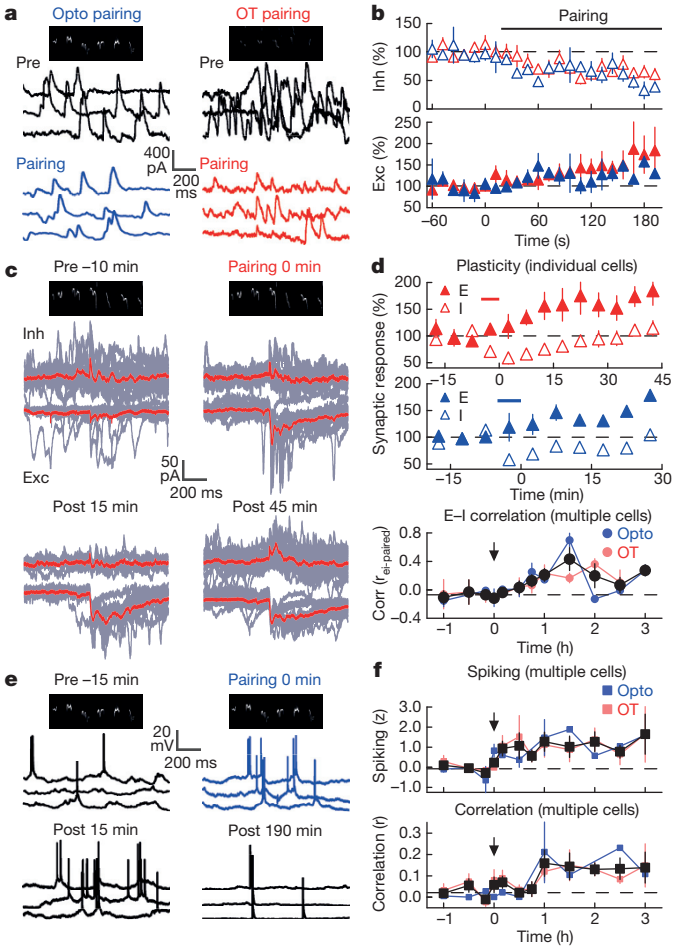

Figure 6 | Oxytocin pairing modifies excitatory–inhibitory balance. **a**, Call-evoked IPSCs from virgin left AI neuron before and during optogenetic (blue) or oxytocin (red) pairing. **b**, Oxytocin reduced inhibition within 40–60 s (top; optogenetic pairing, $n = 4$, $P < 0.002$, Student's paired two-tailed t-test; oxytocin pairing, $n = 12$, $P < 0.04$). **c**, Voltage-clamp recording from virgin left AI neuron (pre-pairing IPSCs: 8.3 ± 1.1 pA, pre-pairing EPSCs: −8.0 ± 1.2 pA, $r_{ei\text{-}paired}$: 0.13; pairing IPSCs: 6.5 ± 1.5 pA, EPSCs: −10.4 ± 3.0 pA, $r_{ei\text{-}paired}$: −0.12; 10–15 min after pairing IPSCs: 4.9 ± 0.9 pA, $P < 0.0009$, EPSCs: −15.4 ± 1.3 pA, $P < 0.005$, $r_{ei\text{-}paired}$: −0.14; 45–50 min after pairing IPSCs: 9.6 ± 2.1 pA, $P > 0.5$, EPSCs: −13.4 ± 2.4 pA, $P < 0.002$, $r_{ei\text{-}paired}$: 0.27). Error bars denote mean ± s.e.m. **d**, Synaptic modifications. Top, individual neurons after oxytocin (EPSC increase: 43.5 ± 15.7%, $n = 10$, $P < 0.03$; IPSC decrease: −33.7 ± 7.8%, $P < 0.004$) or optogenetic pairing (EPSC increase: 47.5 ± 13.2%, $n = 6$, $P < 0.02$; IPSC decrease: −20.0 ± 4.3%, $P < 0.02$). Bottom, excitatory–inhibitory correlation ($n = 28$ cells, 17 animals; $r_{ei\text{-}paired}$ pre-pairing: −0.07 ± 0.05, $r_{ei\text{-}paired}$ 0–45 min after pairing: 0.02 ± 0.04, $P > 0.1$; $r_{ei\text{-}paired}$ 1–3 h post-pairing: 0.24 ± 0.06, $P < 0.0002$). **e**, Two current-clamp recordings from same virgin; first cell before optogenetic pairing (z-score:0.04, r: 0.01), during pairing (z: 0.51, r: 0.00), 10–15 min post-pairing (z: 0.57, r: 0.03); second cell 180–190 min after pairing (z: 1.60, r: 0.11). **f**, Spiking. Top, call-evoked spiking ($n = 28$ cells, 13 animals; z-score pre-pairing: −0.13 ± 0.11, 0–45 min post-pairing: 0.91 ± 0.27, $P < 0.003$; z-score 1–3 h post-pairing: 1.21 ± 0.25, $P < 10^{-4}$). Bottom, trial-by-trial correlation (pre-pairing r: 0.01 ± 0.01; 0–45 min post-pairing: 0.05 ± 0.02, $P > 0.1$; 1–3 h post-pairing: 0.14 ± 0.03, $P < 10^{-4}$).

not naive virgins or the right AI. We quantified the degree of excitatory–inhibitory balance of call-evoked responses three ways: trial-by-trial similarity in patterns of excitatory or inhibitory responses (r_e, r_i), fine-scale correlation of temporal structure between EPSCs and IPSCs from best calls ($r_{ei\text{-}best}$), and overall correlation between EPSC and IPSC amplitudes across all calls ($r_{ei\text{-}all}$). First, we examined synaptic responses to best calls, and found that in experienced animals, patterns of EPSCs and IPSCs were similar and more reliable from trial-to-trial (Extended Data Fig. 6b, e).

For fine-scale excitatory–inhibitory balance, we observed that temporal profiles of call-evoked excitation and inhibition were almost identical in maternal animals. Although we could not simultaneously measure both excitation and inhibition in a given trial, we reasoned that because of similarity between excitation and inhibition alone, average responses would also be correlated. Indeed, temporal correlations of EPSCs and IPSCs evoked by best calls ($r_{ei\text{-}best}$) were higher in the left AI of experienced animals (Fig. 5d and Extended Data Fig. 5c). Finally, for overall correlation across vocalizations, each different call evoked a distinct EPSC/IPSC pattern. In the left AI neurons from

experienced but not naive animals, call-evoked EPSC and IPSC magnitudes were correlated (Fig. 5d and Extended Data Fig. 5c).

Temporal correlation of excitation and inhibition provides a mechanism for reliable and precisely timed spiking responses. As proof of principle, we simulated spiking evoked by different sets of synaptic call-evoked responses in a conductance-based integrate-and-fire model neuron[36]. We computed membrane potential and spiking responses and observed precisely timed spikes in cells from experienced but not naive animals (Extended Data Fig. 7), due to temporal mismatch between excitation and inhibition. Therefore, the patterns of EPSCs and IPSCs in experienced animals can account for reliable spiking observed in the maternal state.

Oxytocin modulation and cortical plasticity

Finally, we wondered how oxytocin sensitized neural circuits of virgin left AI to pup calls, to enable reliable spiking and successful retrieval in initially inexperienced animals. First we examined the neuromodulatory effects of oxytocin on cortical responses *in vivo* and *in vitro*. In voltage-clamp recordings, oxytocin reduced call-evoked IPSCs within seconds (Fig. 6a, b, open; Extended Data Fig. 8). By contrast, EPSCs were gradually modified over minutes (Fig. 6a, b, filled). Therefore, oxytocin rapidly disinhibits the auditory cortex much like acetylcholine[37–40], suggesting that oxytocin may regulate attention and increase the salience of social stimuli. These results corroborate recent findings in hippocampal slices on the effects of oxytocin[41] and oestrogen[42].

We then asked whether repetitive pairing of pup calls in the presence of oxytocin would persistently modify cortical pup call representations, effectively changing the virgin state into the maternal state. After recording responses to pup calls in virgin left AI, we paired calls for 3–5 min with either topical oxytocin application (oxytocin pairing) or optical stimulation of AI in *Oxt*-IRES-Cre animals (optogenetic pairing). A recording demonstrating oxytocin pairing is shown in Fig. 6c (individual trials in Extended Data Fig. 9a). Before pairing, calls evoked unreliable EPSCs and IPSCs. During and after pairing, IPSCs decreased while EPSCs potentiated, becoming more reliable. Forty-five minutes after pairing, however, IPSCs increased in strength and reliability, balancing the temporal profile of inhibition with excitation.

To examine the slower dynamics of inhibitory plasticity after pairing, we made multiple recordings in series after the first recording[36,37]. The correlation of average excitation and inhibition evoked by paired calls ($r_{\text{ei-paired}}$) steadily increased over an hour and was stable thereafter (Fig. 6d). As excitatory modifications and changes in reliability were maximal after 20–30 min, this increase in excitatory–inhibitory balance probably reflects gradual inhibitory potentiation, also evident in changes to inhibitory trial-by-trial correlations after pairing (Extended Data Fig. 9b).

Our simulations (Extended Data Fig. 7) indicated that this delayed balancing of excitation and inhibition has substantial consequences for call-evoked spiking. Specifically, spike timing precision should increase when IPSCs match the pattern of EPSCs. Consistent with this hypothesis, spiking responses were rapidly increased during and after pairing, but trial-by-trial correlations increased only after an hour (Fig. 6f). Thus, briefly pairing pup calls with cortical oxytocin triggers long-lasting changes in virgin AI circuitry, balancing inhibition with excitation to enhance call representation and perceptual salience within minutes to hours.

Discussion

Our results demonstrate a remarkable degree of functional lateralization in the mammalian brain and provide a molecular basis for this phenomenon. The left auditory cortex is specialized for recognizing the behavioural significance of infant distress calls and required for maternal retrieval of isolated pups. This is markedly similar to the asymmetry of speech processing in human temporal lobe[43,44], and supports earlier behavioural observations of auditory lateralization in maternal mice[19]. We generated an antibody to the mouse oxytocin receptor, OXTR-2, and found more receptor expression in the left auditory cortex. A dedicated neural circuit, enriched for oxytocin receptors, might therefore be specialized for processing important social signals such as pup distress calls. This specialization would allow maternal animals to attend to their young and return pups to the nest rapidly and reliably. Furthermore, given the importance of olfactory signals in social behaviours including pup retrieval[13,23,45,46], it is likely that oxytocin also enhances olfaction[47] in combination with other cues (for example, pup calls) to improve parenting behaviour synergistically.

Although many aspects of mammalian maternal behaviour may be innate[48–50], recognition of the behavioural importance of pup calls depends on experience[21,23,25–28]. Several studies highlight differences between AI responses in maternal and pup-naive female mice. In particular, pup call responses have been found to be less reliable in pup-naive virgins[23,25–27]. Our results directly demonstrate how oxytocin paired with pup calls rapidly changes brain state, transforming weaker virgin responses into more robust and temporally precise maternal-like responses. The predominant effect of oxytocin is to reduce cortical inhibition within seconds, followed by longer-term modifications over hours proposed to be essential for balancing inhibition with excitation, enhancing spiking and successful maternal care. These synaptic dynamics are analogous to the imbalance of excitation and inhibition for tone-evoked responses in AI during early development when animals have had limited acoustic exposure[36]. After experience, however, tone-evoked excitation and inhibition become balanced over the first few weeks of life[34–37]. Our findings complement recent studies of neural circuits involved in social behaviour[23,48–50] by revealing how ethologically important behaviours with innate components can be quickly shaped and improved by experience. This may exemplify a general mechanism of neuromodulation for social behaviour.

Online Content Methods, along with any additional Extended Data display items and Source Data, are available in the online version of the paper; references unique to these sections appear only in the online paper.

Received 28 August 2014; accepted 10 March 2015.
Published online 15 April 2015.

1. Richard, P., Moos, F. & Freund-Mercier, M. J. Central effects of oxytocin. *Physiol. Rev.* **71,** 331–370 (1991).
2. Gimpl, G. & Fahrenholz, F. The oxytocin receptor system: structure, function, and regulation. *Physiol. Rev.* **81,** 629–683 (2001).
3. Insel, T. R. & Young, L. J. The neurobiology of attachment. *Nature Rev. Neurosci.* **2,** 129–136 (2001).
4. Insel, T. R. The challenge of translation in social neuroscience: a review of oxytocin, vasopressin, and affiliative behavior. *Neuron* **65,** 768–769 (2010).
5. Bartz, J. A., Zaki, J., Bolger, N. & Ochsner, K. N. Social effects of oxytocin in humans: Context and person matter. *Trends Cogn. Sci.* **15,** 301–309 (2011).
6. Churchland, P. S. & Winkielman, P. Modulating social behavior with oxytocin: how does it work? What does it mean? *Horm. Behav.* **61,** 392–399 (2012).
7. Pedersen, C. A., Ascher, J. A., Monroe, Y. L. & Prange, A. J. Oxytocin induces maternal behavior in virgin female rats. *Science* **216,** 648–650 (1982).
8. Winslow, J. T. & Insel, T. R. Social status in pairs of male squirrel monkeys determines the behavioral response to central oxytocin administration. *J. Neurosci.* **11,** 2032–2038 (1991).
9. Nishimori, K. *et al.* Oxytocin is required for nursing but is not essential for parturition or reproductive behavior. *Proc. Natl Acad. Sci. USA* **93,** 11699–11704 (1996).
10. Zak, P. J., Stanton, A. A. & Ahmadi, S. Oxytocin increases generosity in humans. *PLoS ONE* **2,** e1128 (2007).
11. Andari, E. *et al.* Promoting social behavior with oxytocin in high-functioning autism spectrum disorders. *Proc. Natl Acad. Sci. USA* **107,** 4389–4394 (2010).
12. Chang, S. W. & Platt, M. L. Oxytocin and social cognition in rhesus macaques: Implications for understanding and treating human psychopathology. *Brain Res.* **1580,** 57–68 (2014).
13. Dulac, C., O'Connell, L. A. & Wu, Z. Neural control of maternal and paternal behaviors. *Science* **345,** 765–770 (2014).
14. Rilling, J. K. & Young, L. J. The biology of mammalian parenting and its effects on offspring social development. *Science* **345,** 771–776 (2014).
15. Yoshida, M. *et al.* Evidence that oxytocin exerts anxiolytic effects via oxytocin receptor expressed in serotonergic neurons in mice. *J. Neurosci.* **29,** 2259–2271 (2009).

16. Nakajima, M., Görlich, A. & Heintz, N. Oxytocin modulates female sociosexual behavior through a specific class of prefrontal cortical interneurons. *Cell* **159,** 295–305 (2014).
17. Sewell, G. D. Ultrasonic communication in rodents. *Nature* **227,** 410 (1970).
18. Noirot, E. Ultrasounds and maternal behavior in small rodents. *Dev. Psychobiol.* **5,** 371–387 (1972).
19. Ehret, G. Left hemisphere advantage in the mouse brain for recognizing ultrasonic communication calls. *Nature* **325,** 249–251 (1987).
20. Fichtel, I. & Ehret, G. Perception and recognition discriminated in the mouse auditory cortex by c-Fos staining. *Neuroreport* **10,** 2341–2345 (1999).
21. Ehret, G. Infant rodent ultrasounds – a gate to the understanding of sound communication. *Behav. Genet.* **35,** 19–29 (2005).
22. Crawley, J. N. Behavioral phenotyping strategies for mutant mice. *Neuron* **57,** 809–818 (2008).
23. Cohen, L., Rothschild, G. & Mizrahi, A. Multisensory integration of natural odors and sounds in the auditory cortex. *Neuron* **72,** 357–369 (2011).
24. Hofstetter, K. M. & Ehret, G. The auditory cortex of the mouse: connections of the ultrasonic field. *J. Comp. Neurol.* **323,** 370–386 (1992).
25. Liu, R. C., Linden, J. F. & Schreiner, C. E. Improved cortical entrainment to infant communication calls in mothers compared with virgin mice. *Eur. J. Neurosci.* **23,** 3087–3097 (2006).
26. Liu, R. C. & Schreiner, C. E. Auditory cortical detection and discrimination correlates with communicative significance. *PLoS Biol.* **5,** e173 (2007).
27. Rothschild, G., Cohen, L., Mizrahi, A. & Nelken, I. Elevated correlations in neuronal ensembles of mouse auditory cortex following parturition. *J. Neurosci.* **33,** 12851–12861 (2013).
28. Koch, M. & Ehret, G. Estradiol and parental experience, but not prolactin are necessary for ultrasound recognition and pup-retrieving in the mouse. *Physiol. Behav.* **45,** 771–776 (1989).
29. Irani, B. G. *et al.* Distribution and neurochemical characterization of protein kinase C-theta and -delta in the rodent hypothalamus. *Neuroscience* **170,** 1065–1079 (2010).
30. Wu, Z. *et al.* An obligate role of oxytocin neurons in diet induced energy expenditure. *PLoS ONE* **7,** e45167 (2012).
31. Knobloch, H. S. *et al.* Evoked axonal oxytocin release in the central amygdala attenuates fear response. *Neuron* **73,** 553–566 (2012).
32. Takayanagi, Y. *et al.* Pervasive social deficits, but normal parturition, in oxytocin receptor-deficient mice. *Proc. Natl Acad. Sci. USA* **102,** 16096–16101 (2005).
33. Gong, S. *et al.* A gene expression atlas of the central nervous system based on bacterial artificial chromosomes. *Nature* **425,** 917–925 (2003).
34. Wehr, M. & Zador, A. M. Balanced inhibition underlies tuning and sharpens spike timing in auditory cortex. *Nature* **426,** 442–446 (2003).
35. Tan, A. Y. & Wehr, M. Balanced tone-evoked synaptic excitation and inhibition in mouse auditory cortex. *Neuroscience* **163,** 1302–1315 (2009).
36. Dorrn, A. L., Yuan, K., Barker, A. J., Schreiner, C. E. & Froemke, R. C. Developmental sensory experience balances cortical excitation and inhibition. *Nature* **465,** 932–936 (2010).
37. Froemke, R. C., Merzenich, M. M. & Schreiner, C. E. A synaptic memory trace for cortical receptive field plasticity. *Nature* **450,** 425–429 (2007).
38. Kruglikov, I. & Rudy, B. Perisomatic GABA release and thalamocortical integration onto neocortical excitatory cells are regulated by neuromodulators. *Neuron* **58,** 911–924 (2008).
39. Letzkus, J. J. *et al.* A disinhibitory microcircuit for associative fear learning in the auditory cortex. *Nature* **480,** 331–335 (2011).
40. Froemke, R. C. *et al.* Long-term modification of cortical synapses improves sensory perception. *Nature Neurosci.* **16,** 79–88 (2013).
41. Owen, S. F. *et al.* Oxytocin enhances hippocampal spike transmission by modulating fast-spiking interneurons. *Nature* **500,** 458–462 (2013).
42. Rudick, C. N. & Woolley, C. S. Estrogen regulates functional inhibition of hippocampal CA1 pyramidal cells in the adult female rat. *J. Neurosci.* **21,** 6532–6543 (2001).
43. Loring, D. W. *et al.* Cerebral language lateralization: evidence from intracarotid amobarbital testing. *Neuropsychologia* **28,** 831–838 (1990).
44. Bishop, D. V. Cerebral asymmetry and language development: cause, correlate, or consequence? *Science* **340,** 1230531 (2013).
45. Yoon, H., Enquist, L. W. & Dulac, C. Olfactory inputs to hypothalamic neurons controlling reproduction and fertility. *Cell* **123,** 669–682 (2005).
46. Fraser, E. J. & Shah, N. M. Complex chemosensory control of female reproductive behaviors. *PLoS ONE* **9,** e90368 (2014).
47. Wacker, D. W. & Ludwig, M. Vasopressin, oxytocin, and social odor recognition. *Horm. Behav.* **61,** 259–265 (2012).
48. Lin, D. *et al.* Functional identification of an aggression locus in the mouse hypothalamus. *Nature* **470,** 221–226 (2011).
49. Bennur, S., Tsunada, J., Cohen, Y. E. & Liu, R. C. Understanding the neurophysiological basis of auditory abilities for social communication: a perspective on the value of ethological paradigms. *Hear. Res.* **305,** 3–9 (2013).
50. Wu, Z., Autry, A. E., Bergan, J. F., Watabe-Uchida, M. & Dulac, C. G. Galanin neurons in the medial preoptic area govern parental behavior. *Nature* **509,** 325–330 (2014).

Supplementary Information is available in the online version of the paper.

Acknowledgements We thank V. Azzara, R. Alicka, H. Bernstein, G. Buzsaki, I. Carcea, C. Grosso, M. Insanally, M. Jin, K. Kuchibhotla, B. Y. B. Lau, D. Lin, M. A. Long, N. Lopez, J. Marlin, C. McFarlane, E. Morina, S. Norden, D. Okobi, K. Peng, R. Priya, W. Rashid, L. Rubin, S. Shea, R. M. Sullivan, R. W. Tsien, D. Vallentin, L. J. Young and N. Zaika for comments, discussions and technical assistance, A. Mar and the NYU School of Medicine Behavioral Core for assistance with behavioural analysis, and C. A. Loomis and the NYU School of Medicine Histology Core for assistance with anatomical studies. Oxytocin-IRES-Cre mice were obtained from D. Olson and B. Lowell. Oxytocin receptor knockout mice were obtained from R. W. Tsien. Oxytocin receptor plasmid (pAAV-OXTR) was obtained from L. J. Young. Adeno-associated virus was obtained from the U. Penn Vector Core. S. E. Ross created artwork in Fig. 1a. This work was funded by NIDCD (DC009635, DC12557), a Klingenstein Fellowship, a McKnight Scholarship, a Pew Scholarship, a Sloan Research Fellowship, and a Whitehead Foundation Fellowship (R.C.F.); a Skirball Institute Collaborative Research Award (M.V.C. and R.C.F.); and NIMH (T32; B.J.M.).

Author Contributions B.J.M. conducted behavioural studies and *in vivo* recordings. M.M. conducted anatomical studies. J.A.D. conducted *in vitro* recordings. M.M. and M.V.C. generated OXTR-2. R.C.F. and B.J.M. designed the study. All authors analysed data and wrote the paper.

Author Information Reprints and permissions information is available at www.nature.com/reprints. The authors declare no competing financial interests. Readers are welcome to comment on the online version of the paper. Correspondence and requests for materials should be addressed to R.C.F. (robert.froemke@med.nyu.edu).

METHODS

Behaviour. All procedures were approved under New York University Institutional Animal Care and Use Committee protocols. For measuring pup retrieval, we used 2–4-month-old C57BL/6 mothers or pup-naive virgin female mice. Dams were initially pre-screened to ensure they retrieved pups; ~1% of dams did not retrieve pups and these animals were not used for co-housing. Naive virgins were initially pre-screened for retrieval or pup mauling before co-housing; <30% of naive virgins retrieved at least one pup or mauled pups during pre-screening and these animals were excluded from subsequent behavioural studies.

Each session of testing consisted of a baseline set of 10 trials and a post-injection/infusion set of 10 trials. For baseline testing, animals were placed in a behavioural arena (38 × 30 × 15 cm) containing nesting material. Animals were given at least 20 min to acclimate before each testing session began. Three to six pups ranging from postnatal days 1 to 4 were grouped in a corner of the arena and covered with nesting material. One pup was removed from the nest and placed in an opposite corner of the arena. The experimental female was given ten trials (2 min per trial) to retrieve the displaced pup and return it back to the nest; if the displaced pup was not retrieved within 2 min, the pup was returned to the nest and the trial was scored as a failure. If the pup was successfully retrieved, the time to retrieval was scored. Another pup was then taken out of the nest, placed in an opposite corner, and the next trial was begun. After ten trials, pups were placed back into their home cage with their dam. We used an ultrasonic microphone (Avisoft) to verify that isolated pups vocalized during testing.

For post-injection testing (Fig. 1b–e), virgin females were injected intraperitoneally with oxytocin (20–50 μM in saline, 0.3 ml) or saline (0.3 ml). For post-infusion testing (Fig. 3c), cannulated virgin animals were infused with oxytocin (50 μM in saline, 1.5 μl at 1 μl min^{-1}) or saline (1.5 μl at 1 μl min^{-1}). For animals that were co-housed (Fig. 1b–d), the dam and litter were placed in the arena with the experimental virgin female and the experienced dam was given at least 5–10 min to re-acclimate. Wild-type naive virgins were randomly assigned to different groups (saline or oxytocin, co-housed or isolate) by an experimenter blind to results of data analysis. Dam retrieval rates were tested in the presence of the experimental virgin female. Afterwards, the dam was removed to her home cage and the retrieval rates of the virgin female were reassessed. Virgin female retrieval was then tested as described above, and afterwards the virgin female was returned to her home cage with dam and pups. Best retrieval performance in Fig. 1d was determined from the session with the highest retrieval rate and the session with the fastest retrieval time over all sessions for each animal. Isolated animal retrieval (Fig. 1e) was examined in the absence of an experienced dam. The isolated virgin females were housed separately from dams and pups, and did not come into contact with the dams. Retrieval was tested at the following time points: 1, 3, 6, 12, 18, 24, 36, 48 and 72 h. Power analysis was performed to determine sample size for statistical significance with a power of β: 0.7; these studies required at least six animals, satisfied in the experiments of Fig. 1. Fisher's two-tailed exact test was used for comparing numbers of animals retrieving in each group for Fig. 1c and e as these data were binomial, and Bonferroni correction used to adjust P values for multiple comparisons. Comparisons were made relative to performance of saline-injected virgin females. ANOVA was used to compare retrieval performance in experienced animals in Fig. 1d. For testing the effects of muscimol or oxytocin receptor antagonist infusion, experienced retrievers were placed in the behavioural arena. Animals were given at least 5–10 min to re-acclimate, and baseline retrieval was performed as above. The animal was then infused with muscimol (2.5 mM in saline, 1.5 μl at 1 μl min^{-1}; Fig. 3a, b) or an oxytocin receptor antagonist[51,52]: either OTA (1 μM in saline, 1.5 μl at 1 μl min^{-1}; Fig. 3d, pink line, open circles) or L-368,899 (2.5 mM in saline, 1.5 μl at 1 μl min^{-1}; Fig. 3d, purple line, filled circles). Mice were randomly assigned to different pharmacological groups by an experimenter blind to results of data analysis. Retrieval was reassessed following the infusion. After 24 h, the experimental female was given 10 baseline trials, infused with saline (1.5 μl at 1 μl min^{-1}), and retrieval re-assessed following the infusion ('post' testing). Power analysis was performed to determine sample size for statistical significance with a power of β: 0.7; these studies required at least six animals, satisfied in the experiments of Fig. 3. Wilcoxon's signed-rank matched-pairs tests were used to non-parametrically compare retrieval performance in Fig. 3a, b, d. For comparing number of animals retrieving overall, Fisher's exact test was used (two-tailed for Fig. 3c; one-tailed for Fig. 3a, as all animals initially retrieved and the number of animals retrieving could only stay the same or decrease), comparing oxytocin/optogenetic animals to saline-infused virgin performance.

Stereotaxic viral injections were performed in *Oxt*-IRES-Cre mice[29,30]. Mice were anaesthetized with 0.7–2.5% isoflurane, placed into a stereotaxic apparatus, and a craniotomy performed over PVN (from bregma: 0.72 mm posterior, 0.12 mm lateral, 4.5 mm ventral). Injections were performed with a 5 μl Hamilton syringe and a 33-gauge needle. Cre-inducible pAAV5-EF1α-DIO-ChETA-eYFP virus[53] was injected into PVN 0.1 nl s^{-1} for a final injection volume of 1.2–1.5 μl. An optical fibre ferrule was then implanted either in PVN (4.5 mm ventral) or in electrophysiologically identified AI (100 μm ventral). The craniotomy and implant was sealed with dental cement, and the virus was given a minimum of 2 weeks to express.

Production of oxytocin receptor antibodies. A custom peptide was synthesized based on the mouse oxytocin receptor amino acid sequence: 243-EGSDAAG GAGRAALARVSSVKLISKAKI-270 in the third intracellular loop[54]. This peptide was chosen based on a high level of antigenicity using the Thermo Scientific Antigen Profiler and lack of cross-reactivity. The resulting polyclonal antisera were tested using western blot and immunohistochemistry before being further purified using affinity chromatography.

Specificity was tested via immunohistochemistry in wild-type and oxytocin receptor knockout[32] brain sections and via western blot analysis of HEK293 cells (Invitrogen) expressing oxytocin receptors (pAAV-OXTR plasmid provided by L. J. Young) and protein extracts from mouse brain. HEK cells were tested for mycoplasma around time of use (mid-2013). Lysates were immunoprecipitated and immunoblotted with OXTR-2 to further evaluate specificity of antibody.

For immunohistochemical analysis, wild-type or oxytocin receptor knockout mice were anaesthetized via intraperitoneal injection (0.1 ml per 10 g) of a ketamine–xylazine mixture containing 15 mg ml^{-1} ketamine and 5 mg ml^{-1} xylazine in 0.9% sodium chloride solution. Mice were perfused intracardially with a solution of heparin (1,000 U ml^{-1}) and PBS to prevent clotting, followed by 40 ml per mouse of freshly prepared 4% paraformaldehyde in PBS. After cryoprotection, sections were blocked and incubated with oxytocin receptor primary antibody diluted in PBS to a concentration of 1 μg ml^{-1}. Sections were incubated for 2 days at 4 °C in a moist chamber. Sections were washed with PBS (3 × 15 min at room temperature) in a staining jar and incubated for 1–2 h at room temperature in Alexa-Fluor-conjugated secondary antibodies diluted 1:500 in PBS. Unbound secondary antibodies were washed with PBS (3 × 15 min at room temperature) and sections were incubated for 10 min at room temperature with a Hoechst solution (1:10,000 stock diluted in PBS) for nuclear staining. After a final rinse, the slides were coverslipped using fluoromount G (Southern Biotechnology Associates). The brains of wild-type and knockout animals were processed together to minimize confounding factors, and parallel sections from knockout animals served as controls. For inhibitory marker co-staining, the protocol followed the procedures described above with the addition of a parvalbumin primary antibody (mouse anti-parvalbumin, Swant, 235, 1:1,000) and a somatostatin primary antibody (rat anti-somatostatin, Millipore, MAB354, 1:1,000) in the oxytocin receptor antibody solution. The secondary antibodies used in these experiments were donkey anti-rabbit Alexa 488 (Molecular Probes; 1:500), donkey anti-rat Alexa 555 (Molecular Probes; 1:500), donkey anti-mouse Alexa 647 (Molecular Probes; 1:500). As a control, omission of primary antibody and/or pre-incubation with peptide eliminated immunofluorescent labelling.

Anatomy. OXTR–eGFP mice were created by the GENSAT initiative from a BAC clone containing eGFP upstream of the oxytocin receptor gene[16,33]. Cryopreserved embryos of this line were imported from the Mutant Mouse Regional Resource Centers (MMRRC) and rederived by the NYU transgenic mouse core facility. These mice were on an FVB/N-Swiss Webster background and were bred by mating hemizygous males with wild-type females. Wild-type littermates were used as controls for eGFP antibody staining. The animals were genotyped using a strain-specific protocol provided by the MMRRC using the following primers: *Oxtr* forward: 5′-GCCACACTTTAAAGAGCCTCAA-3′; GFP reverse: 5′-TAG CGGCTGAAGCACTGCA-3′. Note that not all cells natively expressing oxytocin receptors necessarily express the transgene, due to ectopic expression or lack of regulatory elements[55].

Slides were examined and imaged using a Carl Zeiss LSM 700 confocal microscope with four solid-state lasers (405/444, 488, 555, 639 nm) and appropriate filter sets. For imaging sections co-stained with multiple antibodies, we used short-pass 555 nm (Alexa Fluor 488), short-pass 640 nm (Alexa Fluor 555), and long-pass 640 nm (Alexa Fluor 647) photomultiplier tubes. The distribution and number of immunoreactive cells in each section were determined by taking images of wild-type and knockout sections under the same laser power output, pinhole aperture, and gain. Images of left and right auditory cortex in at least three sections per brain were collected and saved for manual counts by two independent blinded observers. Mean numbers of labelled cells were calculated and compared in Fig. 2h by Student's paired two-tailed t-tests as data passed Kolmogorov–Smirnov normality tests. Power analysis was performed to determine sample size for statistical significance with a power of β: 0.7; these studies required at least seven animals, satisfied in the experiments of Fig. 2h. Images of sections costained with inhibitory interneuron markers were collected for each channel and merged to evaluate colocalization with oxytocin receptors by two independent blinded observers. For axon length measurements in

Extended Data Fig. 4d, YFP-positive axon segments from left and right auditory cortex sections in *Oxt*-IRES-Cre animals were quantified with ImageJ by one blinded observer. Four sections spanning anterior to posterior auditory cortex from each animal and each cortical area were examined, and confocal images consisted of a *z*-stack that spanned the thickness of the section. Axon counts were averaged together across the four sections from each animal, and average counts tested for statistical differences with an unpaired two-tailed Student's *t*-test.

Surgical preparation. For *in vivo* electrophysiology or implanting cannulas/ferrules into auditory cortex, female mice were anaesthetized with isoflurane (0.5–2.5%). A small craniotomy was performed over left or right auditory cortex with stereotaxic coordinates (from bregma in mm: 2.9 posterior, 4.0 lateral). To ensure recordings or implants were targeted to AI, we first recorded multiunit activity with tungsten electrodes. AI was mapped with pure tones (60 dB SPL, 7–79 kHz, 50 ms, 1 ms cosine on/off ramps) delivered in pseudo-random sequence at 0.5–1 Hz. For survival surgeries, a cannula or ferrule was then implanted (0.6 mm projection, dummy 0.6 mm projection, internal 0.7 mm projection) using dental acrylic, and animals were given 3–7 days to recover before behavioural testing.

For viral injections, *Oxt*-IRES-Cre animals were bred into a C57BL/6 background. Female mice 2–4 months old were anaesthetized with isoflurane (0.5–2.5%). A craniotomy was performed over the left PVN using stereotaxic coordinates (from bregma in mm: 0.7 posterior, 0.25 lateral, 4 ventral), and pAAV5-EFIα-DIO-ChETA-eYFP (1–1.2 µl) was injected (0.1 µl min^{-1}). Animals were given at least 2 weeks to recover to allow adequate expression of the ChETA variant of channelrhodopsin-2.

Electrophysiology. *In vivo* recordings were performed in a sound-attenuating chamber. Initially, auditory cortex was mapped with multi-unit recordings using a tungsten electrode to determine the tonotopic organization of the primary field AI[24]. After locating AI, *in vivo* whole-cell recordings[34–37] were made from AI neurons with a Multiclamp 700B amplifier (Molecular Devices). For current-clamp recordings, patch pipettes (4–9 MΩ) contained (in mM): 115 K-gluconate, 20 KCl, 1.5 $MgCl_2$, 10 HEPES, 10 phosphocreatine, 2 MgATP, 0.5 NaGTP, pH 7.3. For voltage-clamp recordings, pipettes contained: 130 Cs-methanesulfonate, 1 QX-314, 4 TEA-Cl, 0.5 BAPTA, 4 MgATP, 20 phosphocreatine, 10 HEPES, pH 7.2. Whole-cell recordings from AI neurons were obtained from cells located 420–800 µm below the pial surface. Data were filtered at 5 kHz, digitized at 20 kHz, and analysed with Clampfit 10 (Molecular Devices). Resting potential of AI neurons: -65.4 ± 14.7 mV; series resistance R_s: 33.1 ± 24.4 MΩ; input resistance R_i: 186.1 ± 83.1 MΩ (mean ± s.d.). Recordings were excluded from analysis if R_s or R_i changed >30% compared to the baseline period.

Pup calls were recorded from isolate pups with an ultrasonic microphone, and a library of six calls (1-s duration, maximal intensity of 60 dB SPL) was used for measuring pup call responses. For measuring spiking responses, cell-attached recordings were first high-pass filtered at 100–200 Hz. Spikes were automatically detected in current-clamp or cell-attached recordings by threshold crossing in Clampex 10. Pure tones (50-ms duration, 3-ms cosine on/off ramps) over 4–64 kHz (0.2–1.0 octave steps) were played at 60 dB SPL. Tone-evoked responses were measured in a 50-ms window starting at tone onset and compared to spontaneous activity in the 50 ms before tone onset. Call-evoked responses were measured throughout the call duration plus 200 ms, and compared to spontaneous activity in the 500 ms before call onset, normalized by computing the *z*-scored call-evoked firing rate relative to the spontaneous rate: $z = (\mu_{evoked} - \mu_{spontaneous})/\sigma_{spontaneous}$. Response magnitude in Figs 4 and 5 are shown for the best frequency and best call, in which 'best' is defined as the stimulus that evoked the maximal amount of spiking or excitatory current.

For measuring trial-by-trial similarity of spike trains[56], binary spike trains were smoothed by convolution with a Gaussian filter (σ: 10 ms) and trial-by-trial cross-correlations computed (~10–20 trials per call per cell); all pairwise cross-correlations were then averaged to measure *r* for spiking responses in Figs 4 and 6 and Extended Data Fig. 5. In raster plots of Fig. 4 and Extended Data Fig. 7, yellow events are simply illustrative and indicate spikes that are synchronous within ~10 ms on 50%+ trials. Synaptic responses and trial-by-trial correlations were measured in a similar manner for Figs 5 and 6 and Extended Data Figs 5, 6 and 9, except that responses were measured as the instantaneous current (in pA): the current integral from call onset to 200 ms after call onset (in pA × ms) and divided by the total time (in ms). Synaptic responses were not smoothed before computing zero-lag cross-correlations between all pairs of individual trials. For examining changes in spiking responses and spiking or synaptic correlations over multiple cells in Fig. 6 and Extended Data Fig. 9, measurements were made up to one hour before pairing, and at 10, 30, 45 and 60 min after pairing when possible. Measurements at longer time periods were made whenever subsequent whole-cell recordings were obtained, separated by at least 15 min $cell^{-1}$ thereafter.

For Figs 4 and 5 and Extended Data Figs 5–7, statistics and error bars are reported as medians ± interquartile range for spiking and synaptic responses to pup calls. As these data did not all pass Kolmogorov–Smirnov normality tests, non-parametric Wilcoxon–Mann–Whitney two-sample rank tests were used for comparing pup call responses in experienced animals to virgin animal responses (however, we note that *P* values obtained with Student's two-tailed unpaired *t*-tests were similar, and each of the significant differences reported here were significant under both parametric and non-parametric statistics). Power analysis was performed to determine sample size for statistical significance with a power of β: 0.7; these studies required at least seven neurons for differences in spiking and at least four neurons for differences in synaptic correlations, satisfied in the experiments of Figs 4 and 5 and Extended Data Figs 5 and 6.

For pairing pup calls with exogenous oxytocin, baseline responses to pup calls were recorded for 5–20 min. A non-preferred pup call was then presented for 1–5 min at 0.5–1 Hz in the presence of topically applied oxytocin (50 µM). For pairing calls with endogenous oxytocin release via optogenetic stimulation in *Oxt*-IRES-Cre mice, blue light pulse trains (473 nm wavelength, 10 ms pulse width duration, 30 Hz stimulation frequency, 1 s total pulse train duration) were delivered (final output powers: 10–15 mW mm^{-2} at brain surface). Pup call presentation began at optical pulse train onset. Changes in responses in Fig. 6 and Extended Data Fig. 9 were compared by Student's paired two-tailed *t*-tests as data passed Kolmogorov–Smirnov normality tests. Power analysis was performed to determine sample size for statistical significance with a power of β: 0.7. Modulation experiments of Fig. 6b required at least three neurons for each group, plasticity experiments of Fig. 6d required at least nine neurons for oxytocin pairing and four neurons for optogenetic pairing, and studies of synaptic and spiking correlations of Fig. 6d, f and Extended Data Fig. 9b required at least eleven neurons; these were all satisfied in the experiments of Fig. 6 and Extended Data Fig. 9.

In vitro recordings were performed in auditory cortex slices prepared from adult C57Bl/6 wild-type or *Oxt*-IRES-Cre mice. Animals were deeply anaesthetized with a 1:1 ketamine:xylazine cocktail and decapitated. The brain was rapidly placed in ice-cold dissection buffer containing (in mM): 87 NaCl, 75 sucrose, 2 KCl, 1.25 NaH_2PO_4, 0.5 $CaCl_2$, 7 $MgCl_2$, 25 $NaHCO_3$, 1.3 ascorbic acid and 10 dextrose, bubbled with 95%/5% O_2/CO_2 (pH 7.4). Slices (300–400 µm thick) were prepared with a vibratome (Leica), placed in warm dissection buffer (33–35 °C) for <30 min, then transferred to a holding chamber containing artificial cerebrospinal fluid at room temperature (ACSF, in mM: 124 NaCl, 2.5 KCl, 1.5 $MgSO_4$, 1.25 NaH_2PO_4, 2.5 $CaCl_2$ and 26 $NaHCO_3$,). Slices were kept at room temperature (22–24 °C) for at least 30 min before use. For experiments, slices were transferred to the recording chamber and perfused (2–2.5 ml min^{-1}) with oxygenated ACSF at 33 °C. Whole-cell voltage-clamp recordings were made from layer 5 pyramidal cells with an Multiclamp 700B amplifier (Molecular Devices) using IR-DIC video microscopy (Olympus). Patch pipettes (3–8 MΩ) were filled with intracellular solution (in mM: 130 Cs-methanesulfonate, 1 QX-314, 4 TEA-Cl, 0.5 BAPTA, 4 MgATP, 20 phosphocreatine, 10 HEPES, pH 7.2). Data were filtered at 2 kHz, digitized at 10 kHz, and analysed with Clampfit 10 (Molecular Devices). Recordings were excluded from analysis if R_s or R_i changed >30% compared to baseline. Focal extracellular stimulation (0.01–1.0 ms, 5–150 µA) was applied with a bipolar glass electrode 100–150 µm from the recording electrode. Mean peak IPSCs were measured in a 5–10-ms window. Changes in IPSCs were compared by Student's unpaired two-tailed *t*-tests as data passed Kolmogorov–Smirnov normality tests. Power analysis was performed to determine sample size with a power of β: 0.6; these studies required at least three neurons, satisfied in the experiments of Extended Data Fig. 8d.

Simulations. The simulations in Extended Data Fig. 7 used a conductance-based integrate-and-fire model neuron similar to our previous study relating synaptic currents and spike generation[36]. For simulating the spiking patterns of each cell, we used EPSCs and IPSCs from Fig. 5b. On each trial, one 1.4-s EPSC and one 1.4-s IPSC were randomly chosen from the set of recorded responses. Excitatory and inhibitory synaptic conductances (g_e and g_i, respectively) were computed from currents as previously described[34–37], and then g_e and g_i were randomly rescaled on each trial to have peak instantaneous conductance over the range 1.0–1.7 nS. Membrane voltage was computed as: $\tau_m \frac{dV}{dt} = V_{rest} - V + g_e(t)(E_e - V) + g_i(t)(E_i - V)$, with $\tau_m = 10$ ms, resting membrane potential $V_{rest} = -70$ mV, excitatory reversal potential $E_e = 0$ mV, and inhibitory reversal potential

$E_i = -70$ mV. A spike was evoked in the postsynaptic neuron if the membrane voltage reached threshold of −40 mV, at which point the membrane potential was set to −80 mV in the next time step. Spike rates and trial-by-trial correlation were determined over 25 trials (approximately the number of trials used for measuring these values in the experiments), and 12 representative trials are displayed in Extended Data Fig. 7a–c for each simulation. Code can be obtained at: http://froemkelab.med.nyu.edu/marlin_etal_simulations.

51. Huber, D., Veinante, P. & Stoop, R. Vasopressin and oxytocin excite distinct neuronal populations in the central amygdala. *Science* **308,** 245–248 (2005).
52. Dölen, G., Darvishzadeh, A., Huang, K. W. & Malenka, R. C. Social reward requires coordinated activity of nucleus accumbens oxytocin and serotonin. *Nature* **501,** 179–184 (2013).
53. Gunaydin, L. A. *et al.* Ultrafast optogenetic control. *Nature Neurosci.* **13,** 387–392 (2010).
54. Kubota, Y. *et al.* Structure and expression of the mouse oxytocin receptor gene. *Mol. Cell. Endocrinol.* **124,** 25–32 (1996).
55. Harris, J. A. *et al.* Anatomical characterization of Cre driver mice for neural circuit mapping and manipulation. *Front. Neural Circuits* **8,** 76 (2014).
56. Fellous, J. M., Tiesinga, P. H., Thomas, P. J. & Sejnowski, T. J. Discovering spike patterns in neuronal responses. *J. Neurosci.* **24,** 2989–3001 (2004).

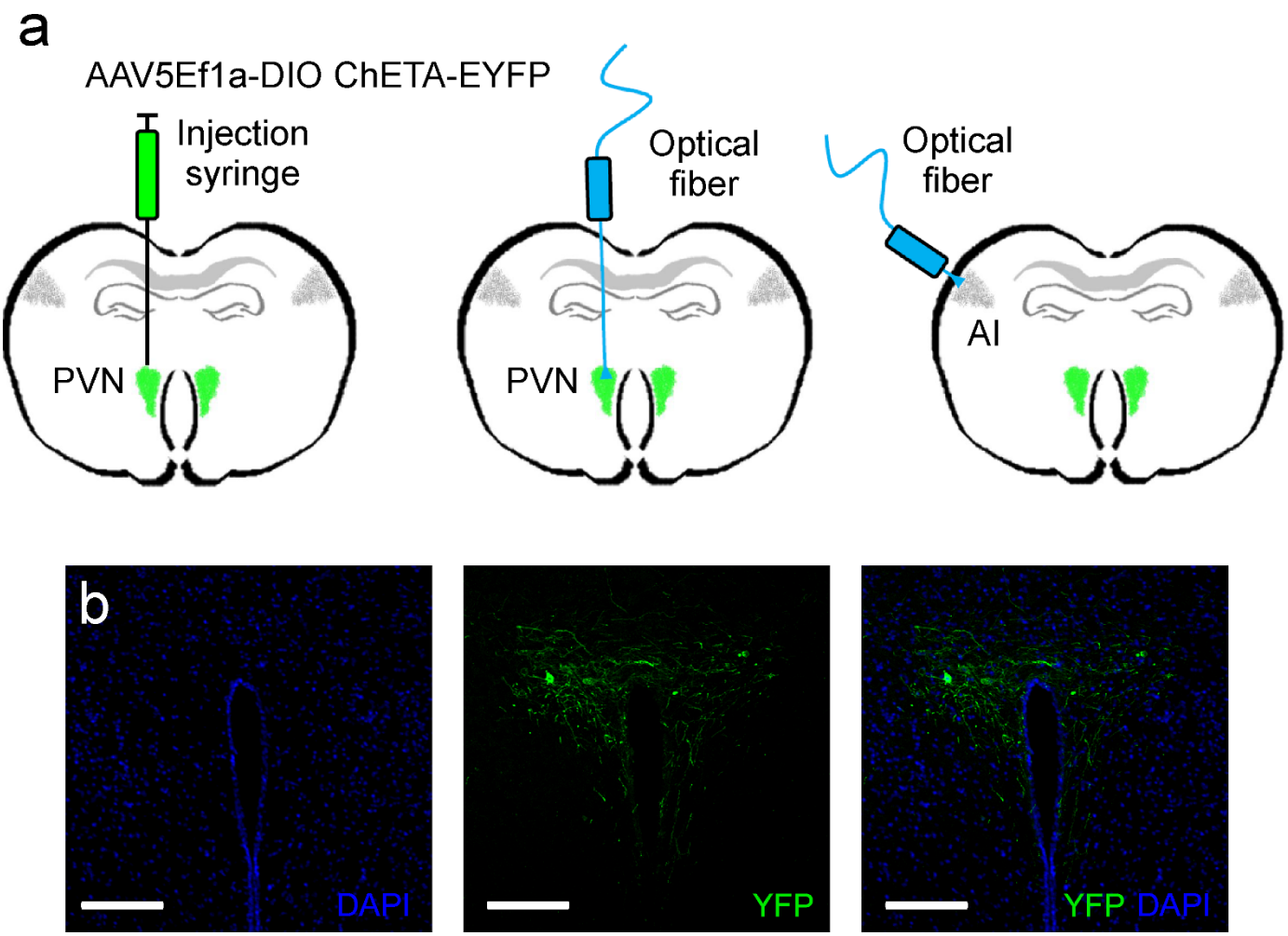

Extended Data Figure 1 | Expression of ChETA in oxytocinergic PVN neurons of *Oxt*-IRES-Cre animals. **a**, Preparation of *Oxt*-IRES-Cre mice for optogenetic stimulation of endogenous oxytocin release. Animals had an adeno-associated virus (AAV) expressing the ChETA variant of channelrhodopsin-2 and YFP (pAAV5-EF1α-DIO-ChETA-eYFP) stereotaxically injected into the left PVN (left) and cannulas for fibre optic stimulation implanted either in the PVN (middle) or left AI (right). **b**, Confirmation of viral expression in PVN. Green, YFP; blue, DAPI. Scale bars, 100 μm.

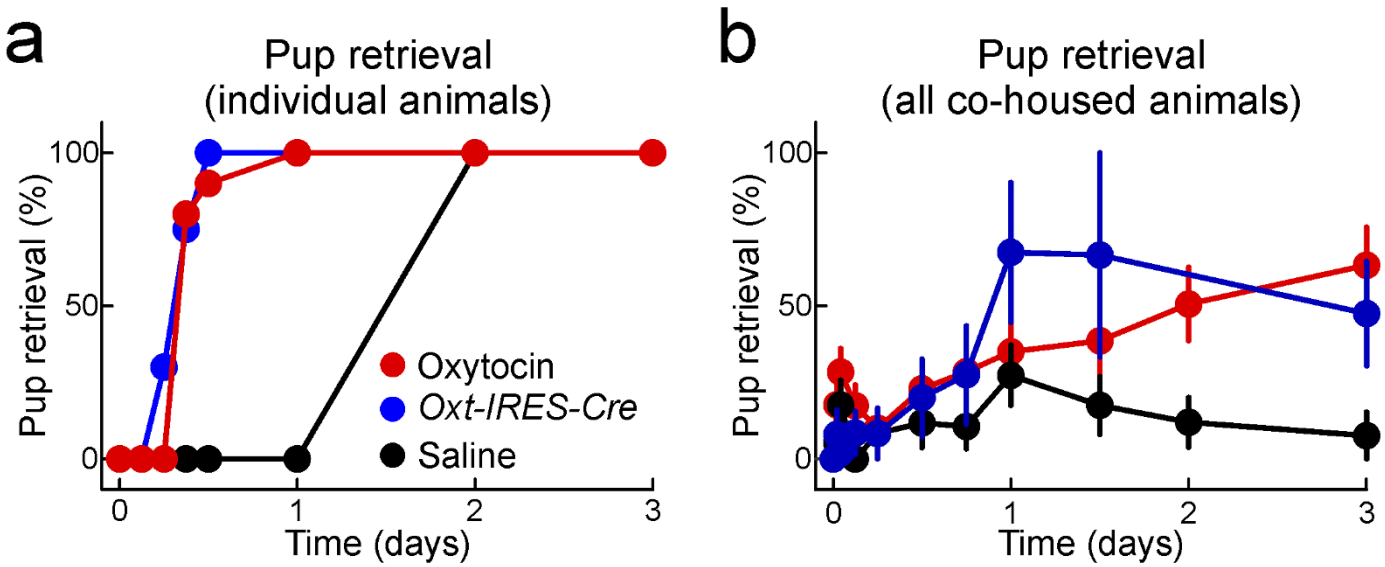

Extended Data Figure 2 | Retrieval success rates over time. **a**, Examples of retrieval rate from three different virgin females receiving optogenetic stimulation of PVN (blue), oxytocin injections (red) or saline injections (black). Each data point is the average over 10 2-min trials immediately after injection or optical stimulation. **b**, Mean retrieval success at each time point for all co-housed virgin animals (including those that never retrieved within the first 3 days of co-housing). Some animals that began retrieving at earlier time points were not assessed at later time points and instead used for electrophysiological experiments.

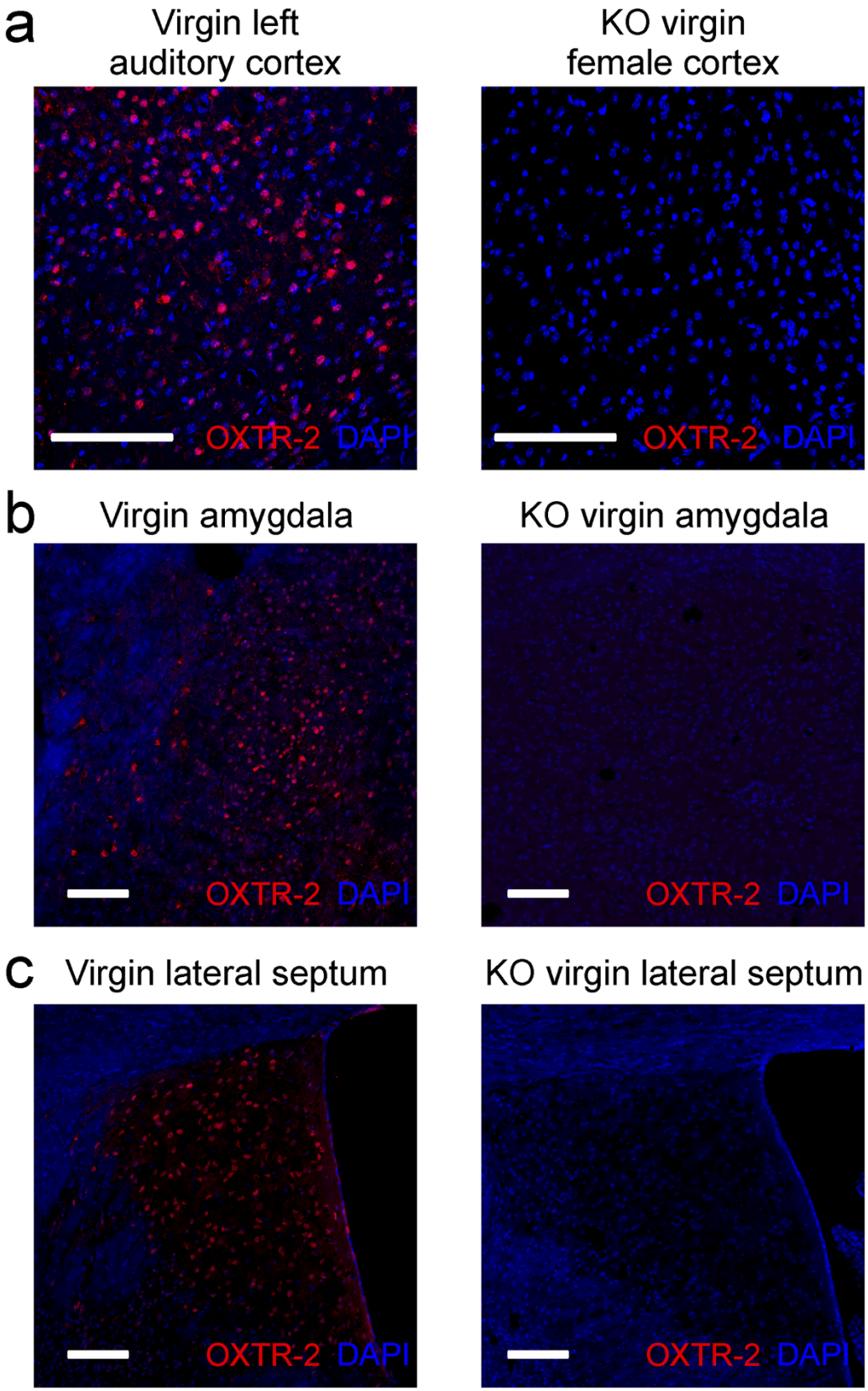

Extended Data Figure 3 | Oxytocin receptor expression in virgin female mouse auditory cortex, amygdala and lateral septum. OXTR-2 labelling was detected in each area in wild-type but not oxytocin receptor knockout animals. **a**, Oxytocin receptor expression measured with OXTR-2 immunostaining in layer 5 of the left auditory cortex of naive wild-type animal (left) or oxytocin receptor knockout animal (right), imaged at ×20 magnification. Red, OXTR-2; blue, DAPI. **b**, OXTR-2 immunostaining in amygdala of wild-type animal (left) or oxytocin receptor knockout animal (right), imaged at ×10 magnification. **c**, OXTR-2 immunostaining in lateral septum of wild-type animal (left) or oxytocin receptor knockout animal (right), imaged at ×10 magnification. Scale bars, 100 μm.

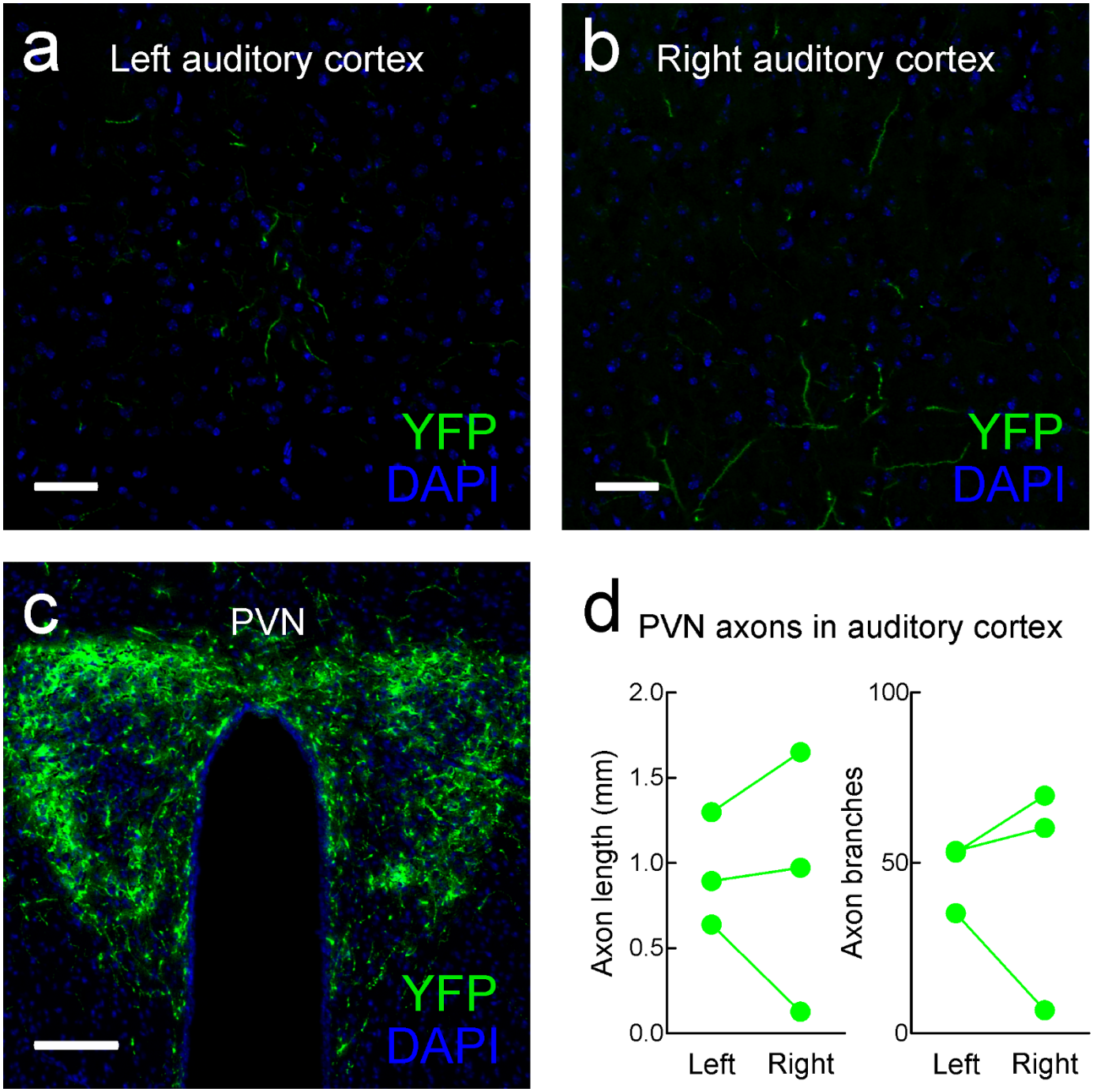

Extended Data Figure 4 | Oxytocinergic projections from hypothalamus to auditory cortex. We identified YFP-positive axon segments in sections from *Oxt*-IRES-Cre animals. **a**, Oxytocinergic projections in left auditory cortex. Green, YFP; blue, DAPI. **b**, Oxytocinergic projections in right auditory cortex from same animal as in **a**. **c**, Oxytocinergic fibres and cells in PVN from same animal as in **a** and **b**. **d**, Quantification of axon segment length and number of axonal branches in left and right auditory cortex. No significant differences were found in total length or branch number in left vs. right cortex (left axon length: 0.94 ± 0.19 mm, right axon length: 0.92 ± 0.44 mm, $n = 3$ mice, $P > 0.9$, Student's paired two-tailed t-test; left: 47.3 ± 6.0 mm axon branches, right: 45.6 ± 19.6 axon branches, $P > 0.9$). Scale bars, 100 μm.

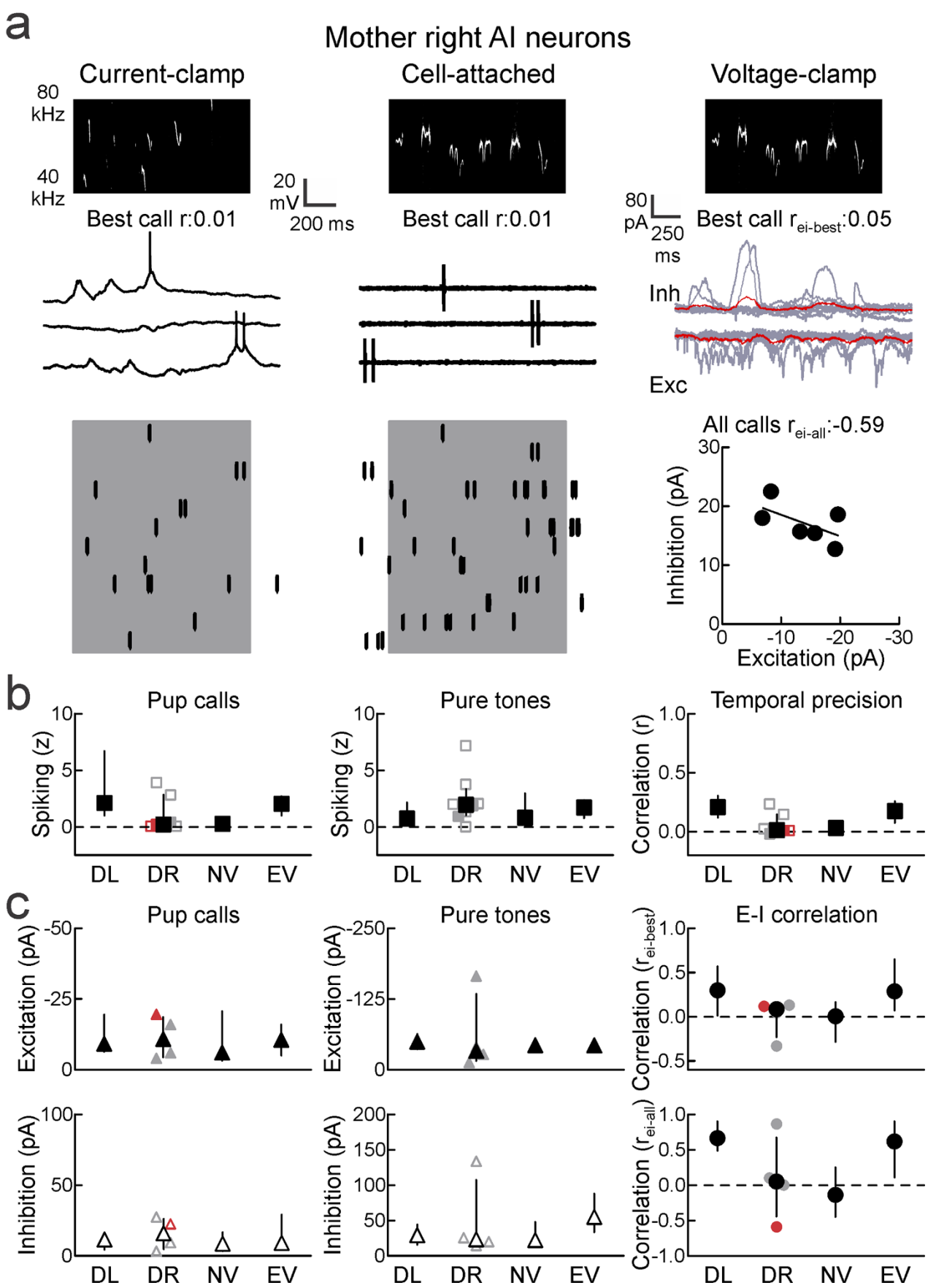

Extended Data Figure 5 | Spiking and synaptic pup call responses in dam right AI neurons. **a**, Three example recordings from right AI neurons of experienced mothers. Left, current-clamp recording. Top, spectrogram of best pup call; middle, three example traces evoked by this call; bottom, raster plot showing spikes evoked over 12 trials (spiking *z*-score: 0.2; trial-by-trial average correlation *r*: 0.01). Middle, cell-attached recording (spiking *z*-score: 0.1; trial-by-trial correlation *r*: 0.01). Right, voltage-clamp recording. IPSCs and EPSCs shown were evoked by the best pup call (grey, individual trials; red, average; $r_{ei\text{-}best}$: 0.05, $r_{ei\text{-}all}$: −0.59). **b**, Summary of spiking responses in dam right (DR) AI neurons. Shown for comparison are responses from left AI neurons of dams (DL), naive virgins (NV), and experienced virgins (EV) from Fig. 4. Left, spiking responses to best pup calls (grey filled squares, current-clamp; open grey squares, cell-attached recordings; black squares, median *z*-score: 0.2 ± 0.8 (median ± s.e.m.), $n = 7$, $P > 0.7$ compared to naive virgin responses with Wilcoxon–Mann–Whitney two-sample rank test with Bonferroni correction for multiple comparisons, $U = 76$). Middle, spiking responses to pure tones (median *z*-score: 1.6 ± 0.3, $n = 8$, $P > 0.4$ compared to naive virgin responses, $U = 83$). Right, trial-by-trial correlation of pup call spiking responses (median *r*: 0.01 ± 0.04, $n = 7$, $P > 0.6$ compared to naive virgin responses, $U = 78$). Red squares indicate cells shown in **a**. **c**, Summary of synaptic responses in dam right AI neurons. Shown for comparison are responses from left AI neurons of dams, naive virgins, and experienced virgins from Fig. 5. Top left, EPSCs evoked by best pup calls (median EPSC: −11.0 ± 4.7, $n = 4$, $P > 0.8$ compared to naive virgin responses, U = 60). Bottom left, IPSCs evoked by best pup calls (median IPSC: 16.0 ± 7.0, $n = 4$, $P > 0.4$ compared to naive virgin responses, $U = 68$). Top middle, EPSCs evoked by pure tones (median EPSC: −33.8 ± 44.1, $n = 7$, $P > 0.4$ compared to naive virgin responses, $U = 52$). Bottom middle, IPSCs evoked by pure tones (median IPSC: 22.9 ± 35.7, $n = 7$, $P > 0.7$ compared to naive virgin responses, $U = 45$). Top right, excitatory–inhibitory correlations in temporal profiles of best call responses (median $r_{ei\text{-}best}$: 0.08 ± 0.14, $n = 4$, $P > 0.7$ compared to naive virgin responses, U = 60). Bottom right, excitatory–inhibitory correlations across all calls (median $r_{ei\text{-}all}$: 0.05 ± 0.37, $n = 4$, $P > 0.8$ compared to naive virgin responses, $U = 59$). Red triangles indicate cell shown in **a**. Error bars denote median ± interquartile range.

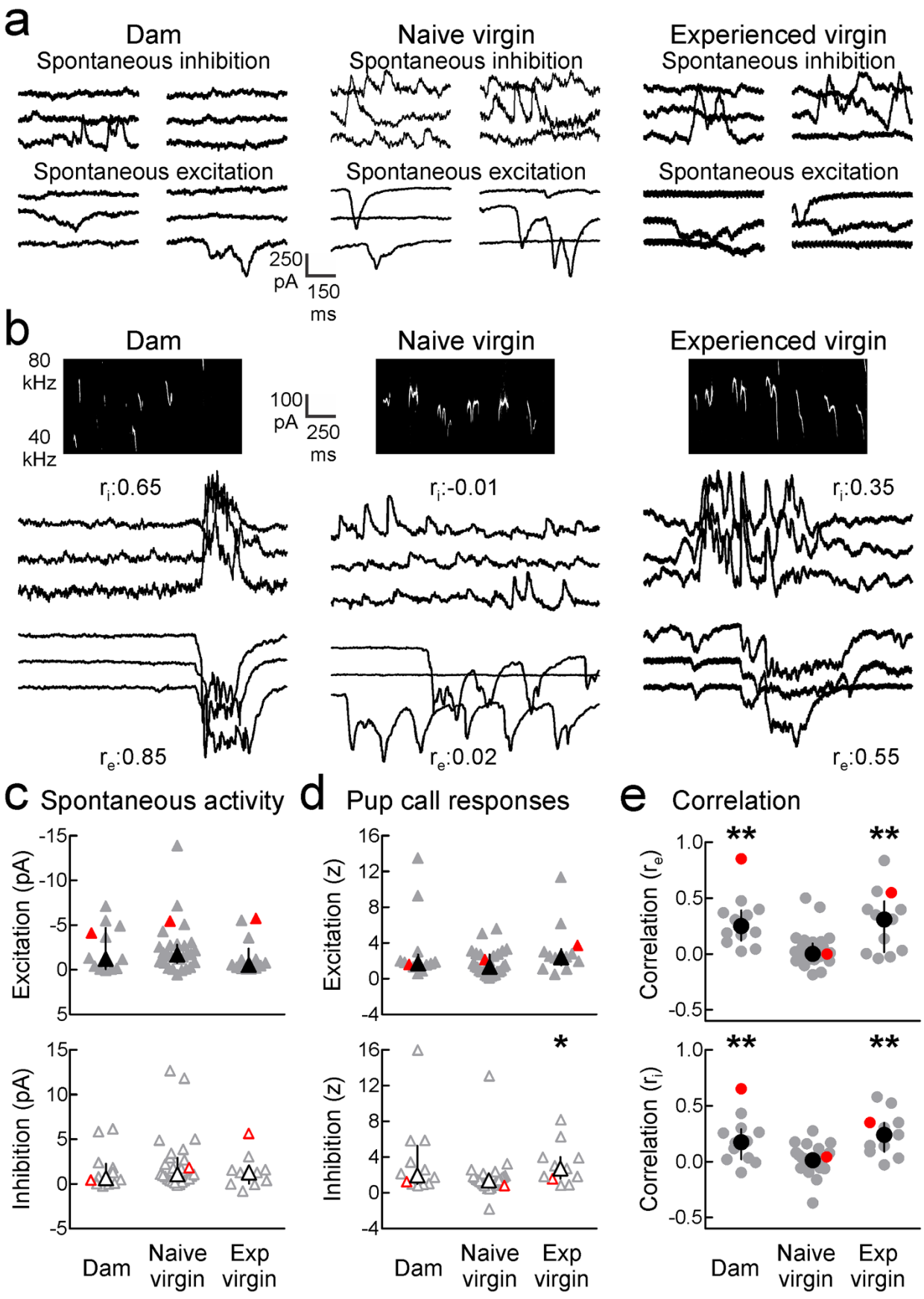

Extended Data Figure 6 | Pup call responses in experienced versus naive females differ in timing but not overall amplitude. **a**, Example periods of spontaneous excitation and inhibition in absence of pup call stimuli; same recordings as in Fig. 5a. **b**, Example call-evoked IPSCs and EPSCs from left AI neurons; same recordings as in Fig. 5a. Left column, neuron from dam. Top, spectrogram. Middle, IPSCs evoked by the best pup call (three individual trials are shown; average trial-by-trial correlation across all trials r_i: 0.65). Note similarity and shared temporal structure across individual trials in this cell. Bottom, EPSCs evoked by this call (r_e: 0.85). Middle column, neuron from naive virgin (r_i: −0.01; r_e: 0.02). Right column, neuron from experienced virgin (r_i: 0.35; r_e: 0.55). **c**, Summary of spontaneous excitation (top, filled triangles) and inhibition (bottom, open triangles) measured as instantaneous current (pA). Spontaneous activity was similar in left AI neurons from dams (black triangle, median excitation: -1.2 ± 0.9 pA (median ± s.e.m.), $n = 13$, $P > 0.7$ compared to naive virgin spontaneous activity with Wilcoxon–Mann–Whitney two-sample rank test with Bonferroni correction for multiple comparisons, $U = 178$; open triangle, median inhibition: 0.6 ± 0.8 pA, $P > 0.3$ compared to naive virgin responses, $U = 193$), naive virgins (median excitation: -1.7 ± 0.7 pA, $n = 28$; median inhibition: 1.1 ± 0.8 pA), and experienced virgins (median excitation: -0.6 ± 0.7 pA, $n = 13$, $P > 0.1$ compared to naive virgin spontaneous activity, $U = 232$; median inhibition: 1.3 ± 0.7 pA, $P > 0.5$ compared to naive virgin responses, $U = 168$). Red triangles indicate cells shown in **a** and **b**. **d**, Summary of z-scored call-evoked EPSCs (top) and IPSCs (bottom) relative to spontaneous activity in dams (filled triangle, median excitation z-score: 1.8 ± 1.4, $n = 13$, $P > 0.1$ compared to naive virgin responses, $U = 215$; open triangle, median inhibition z-score: 2.0 ± 1.6, $P > 0.1$ compared to naive virgin responses, $U = 181$), naive virgins (median excitation z-score: 1.4 ± 0.3, $n = 28$; median inhibition z-score: 1.4 ± 0.6), and experienced virgins (median excitation z-score: 2.5 ± 1.0, $n = 13$, $P > 0.1$ compared to naive virgin responses, $U = 250$; median inhibition z-score: 2.7 ± 0.9, $P < 0.02$ compared to naive virgin responses, $U = 228$). Red triangles indicate cells shown in **a** and **b**. **e**, Summary of trial-by-trial correlations in temporal profile of best call responses for EPSCs (top, r_e) and IPSCs (bottom, r_i) for dams (r_e: 0.25 ± 0.08, $n = 12$, $P < 10^{-4}$ compared to naive virgin responses, $U = 294$; r_i: 0.18 ± 0.08, $P < 0.01$ compared to naive virgin responses, $U = 230$), naive virgins (r_e: 0.0 ± 0.03, $n = 28$; r_i: 0.01 ± 0.03), and experienced virgins (r_e: 0.31 ± 0.09, $n = 13$, $P < 0.007$ compared to naive virgin responses, $U = 285$; r_i: 0.24 ± 0.07, $P < 0.001$ compared to naive virgin responses, $U = 233$). Red circles indicate cells shown in **a** and **b**. $^*P < 0.05$, $^{**}P < 0.01$. Error bars are median ± interquartile range.

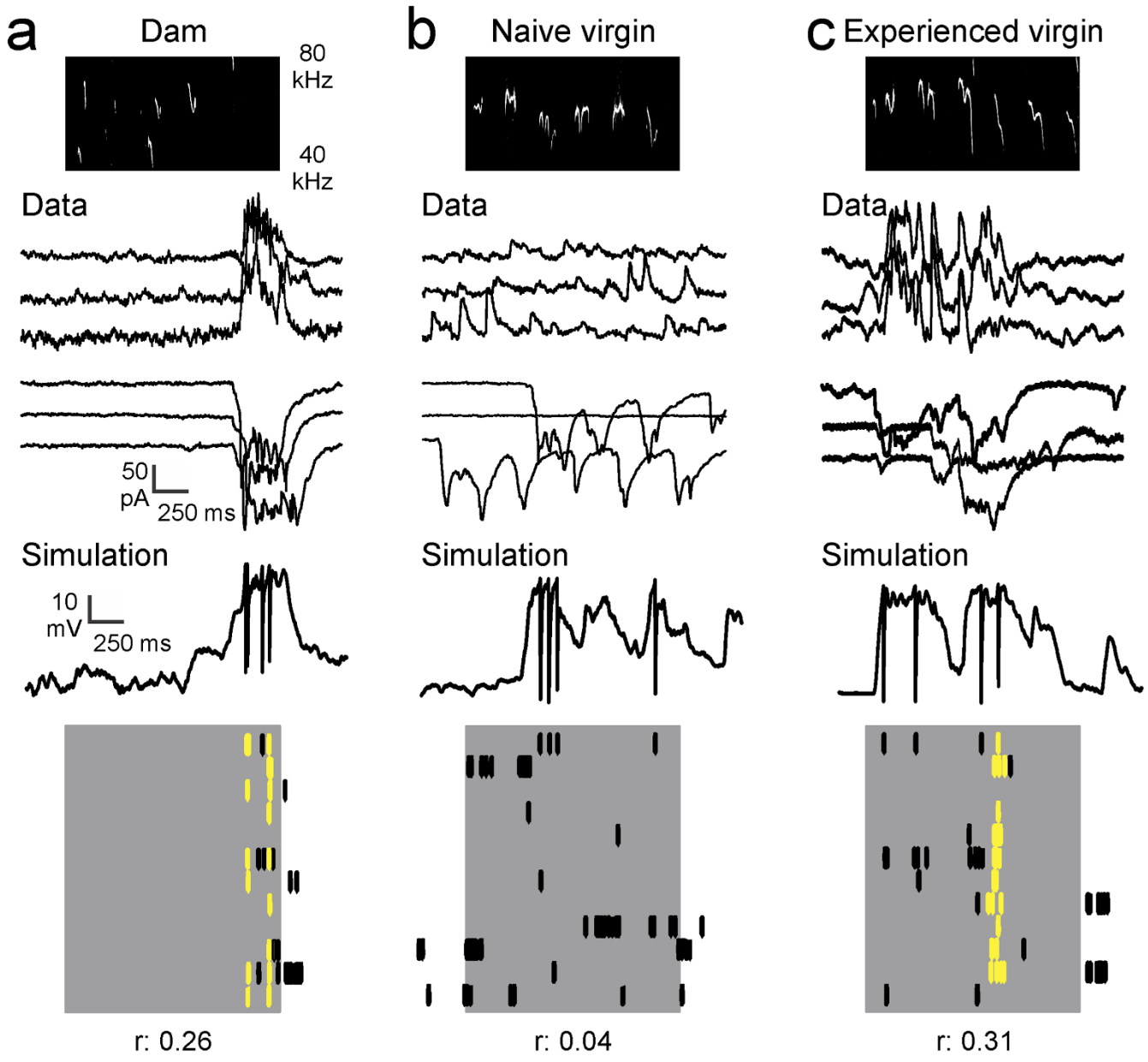

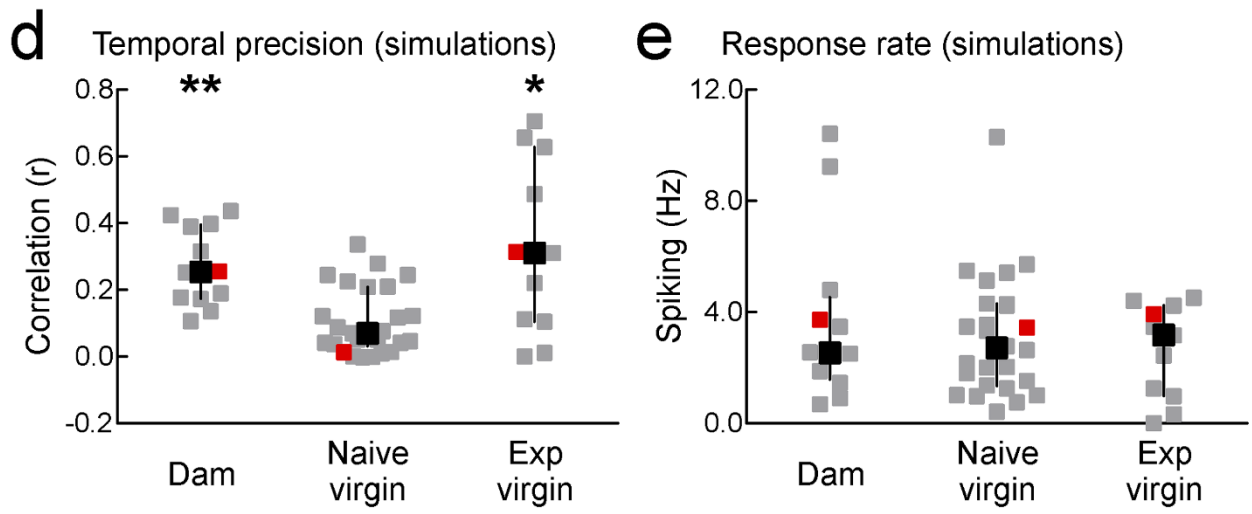

Extended Data Figure 7 | Simulations of spikes predicted from currents measured in voltage-clamp recordings. **a**, Neuron from dam left AI (same cell as in Fig. 5a, left). Top, experimental data. Three representative EPSCs and three IPSCs evoked by the best call are displayed. Bottom, results of simulation. The membrane potential and spikes (clipped for display) of one trial run is shown, with a raster plot of 12 trials below. Yellow events indicate spikes that are synchronous within ~10 ms on 50%+ trials. There was a high trial-to-trial correlation in spike firing (r: 0.26). **b**, Neuron from naive virgin left AI (same cell as in Fig. 5a, middle). Simulations using currents recorded in this cell predicted a low trial-to-trial correlation (r: 0.04). **c**, Neuron from experienced virgin left AI (same cell as in Fig. 5a, right). Simulations predicted a high trial-to-trial correlation (r: 0.31). **d**, Summary of simulated trial-by-trial spiking correlations for all voltage-clamp recordings from Fig. 5 of dams (r: 0.25 ± 0.04 (median ± s.e.m), $n = 12$, $P < 0.0004$ compared to simulated naive virgin responses with Wilcoxon–Mann–Whitney two-sample rank test with Bonferroni correction for multiple comparisons, $U = 269$), naive virgins (median r: 0.07 ± 0.02, $n = 26$), and experienced virgins (median r: 0.31 ± 0.10, $n = 11$, $P < 0.04$ compared to simulated naive virgin responses, $U = 213$). Red squares indicate cells shown in **a**–**c**. Note similarity to spike timing correlations measured experimentally and shown in Fig. 4e. $^{**}P < 0.01$; $^{*}P < 0.05$. **e**, Summary of simulated call-evoked firing rates of dams (median: 2.5 ± 1.1 Hz, $n = 12$, $P > 0.8$ compared to naive virgin responses, $U = 161$), naive virgins (median: 2.7 ± 0.5 Hz, $n = 23$), and experienced virgins (median: 3.2 ± 0.6 Hz, $n = 11$, $P > 0.6$ compared to naive virgin responses, $U = 157$). The simulated call-evoked responses were similar across each group due to the normalization of evoked current amplitudes; normalizing peak EPSCs and IPSCs allowed us to examine changes in spike timing independently from changes in overall spike rate. Error bars are median ± interquartile range.

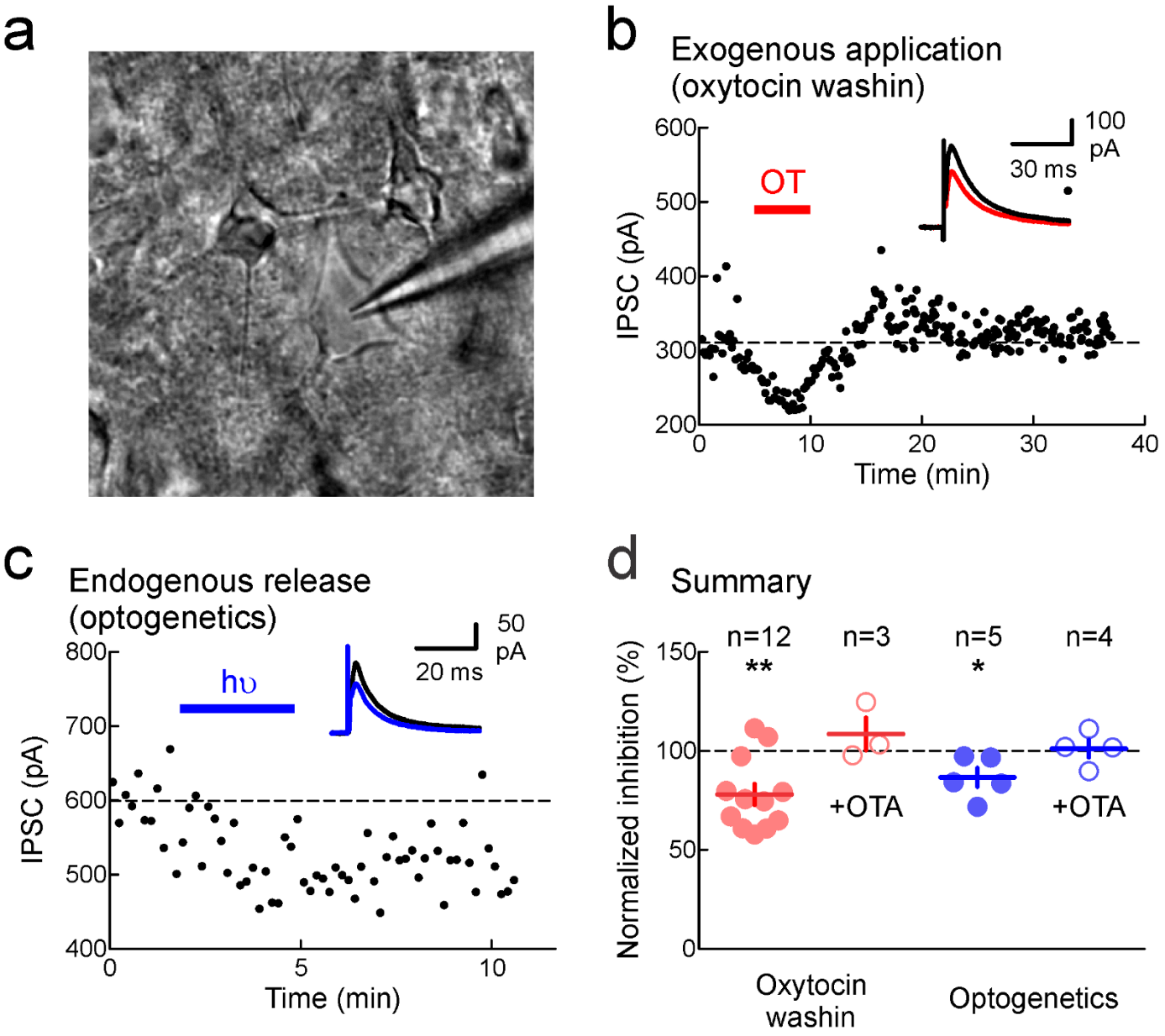

Extended Data Figure 8 | Oxytocin receptor activation disinhibits cortical neurons in brain slices. **a**, Photomicrograph showing whole-cell recording from layer 5 pyramidal neuron in brain slice of virgin female mouse auditory cortex. **b**, Example voltage-clamp recording of IPSCs evoked by extracellular stimulation. Oxytocin was washed into the bath for 5 min. Red bar, duration of oxytocin wash-in. Dashed line, baseline IPSC amplitude. $^{**}P < 0.01$. Inset, IPSCs before (black) and 3–5 min after wash-in (red). **c**, Example voltage-clamp recording of IPSCs evoked by extracellular stimulation in brain slice from *Oxt*-IRES-Cre mouse expressing ChETA in oxytocin neurons. Oxytocin release was evoked by blue light (hυ) for 3 min. $^{*}P < 0.05$. **d**, Summary of changes to evoked IPSCs 3–5 min after oxytocin receptor activation, by exogenous oxytocin wash-in (red; 78.0 ± 5.3% (mean ± s.e.m.) of baseline amplitude; $n = 12$, $P < 0.002$ compared to baseline with Student's two-tailed paired *t*-test; prevented by OTA, 108.6 ± 8.6% of baseline amplitude; $n = 3$, $P > 0.4$ compared to baseline) or by optogenetic release of endogenous oxytocin (86.7 ± 4.7% of baseline amplitude; $n = 5$, $P < 0.05$ compared to baseline; prevented by OTA, 101.2 ± 1.2% of baseline amplitude; $n = 4$, $P > 0.8$ compared to baseline). Error bars are mean ± s.e.m.

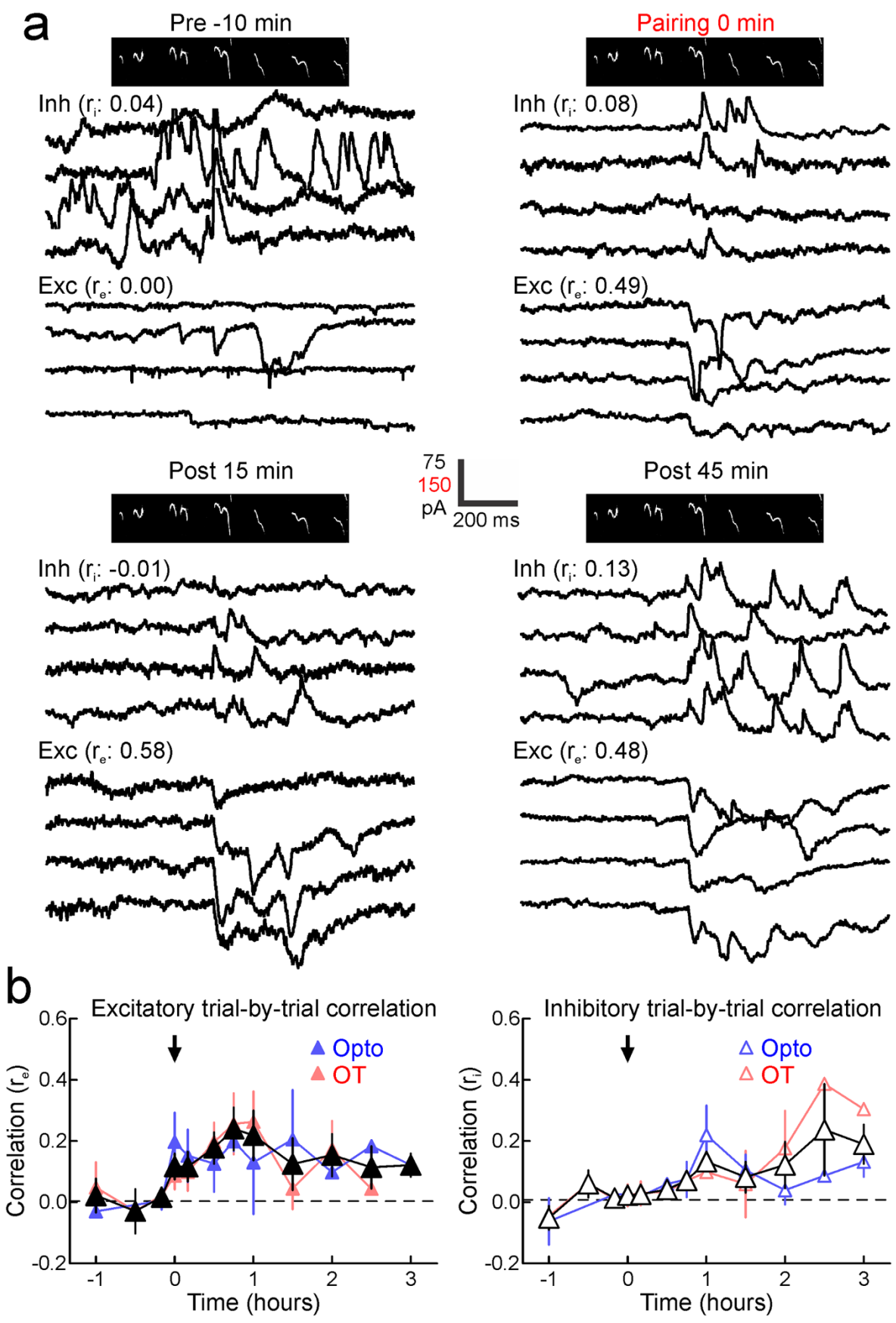

Extended Data Figure 9 | Oxytocin pairing increases the trial-by-trial similarity of synaptic pup call responses. **a**, Same voltage-clamp recording from virgin female left AI neuron as in Fig. 6c, showing that trial-by-trial similarity of call-evoked IPSCs and EPSCs is initially low but increases after oxytocin pairing. Shown are four representative IPSCs and EPSCs before pairing (inhibitory trial-by-trial correlation r_i: 0.04, excitatory trial-by-trial correlation r_e: 0.00), during pairing (r_i: 0.08, r_e: 0.49), 10–15 min after pairing (r_i: −0.01, r_e: 0.58), and 45–50 min after pairing (r_i: 0.13, r_e: 0.48). Scale bar, 75 pA (150 pA during pairing), 200 ms. **b**, Summary of changes to synaptic trial-by-trial correlations after oxytocin pairing in virgin left AI. Left, change in excitatory correlations (r_e) across multiple cells for hours after pairing. Blue, optogenetic pairing; red, oxytocin pairing; black, means binned over time ($n = 28$ cells from 17 animals; r_e before pairing: 0.01 ± 0.02 (mean ± s.e.m.), r_e 0–45 min after pairing: 0.16 ± 0.03, $P < 0.0002$ compared to values before pairing; r_e 1–3 h after pairing: 0.16 ± 0.04, $P < 0.0009$ compared to values before pairing). Dashed line, initial average r_e; arrow, time of pairing. Right, change in r_i (r_i before pairing: 0.01 ± 0.02, r_i 0–45 min after pairing: 0.04 ± 0.02, $P > 0.1$ compared to values before pairing; r_i 1–3 h after pairing: 0.14 ± 0.03, $P < 0.0002$ compared to values before pairing). Error bars are mean ± s.e.m.